UCRL-17003

University of California

Ernest O. Lawrence Radiation Laboratory

K^+p INELASTIC INTERACTIONS AT 2.7 BeV/c

TWO-WEEK LOAN COPY

This is a Library Circulating Copy which may be borrowed for two weeks. For a personal retention copy, call Tech. Info. Division, Ext. 5545

Berkeley, California

DISCLAIMER

This document was prepared as an account of work sponsored by the United States Government. While this document is believed to contain correct information, neither the United States Government nor any agency thereof, nor the Regents of the University of California, nor any of their employees, makes any warranty, express or implied, or assumes any legal responsibility for the accuracy, completeness, or usefulness of any information, apparatus, product, or process disclosed, or represents that its use would not infringe privately owned rights. Reference herein to any specific commercial product, process, or service by its trade name, trademark, manufacturer, or otherwise, does not necessarily constitute or imply its endorsement, recommendation, or favoring by the United States Government or any agency thereof, or the Regents of the University of California. The views and opinions of authors expressed herein do not necessarily state or reflect those of the United States Government or any agency thereof or the Regents of the University of California.

Research and Development

UCRL-17003

UNIVERSITY OF CALIFORNIA

Lawrence Radiation Laboratory
Berkeley, California

AEC Contract No. W-7405-eng-48

K^+p INELASTIC INTERACTIONS AT 2.7 BeV/c

Riley David Newman

PH D THESIS

July 1966

K^+p INELASTIC INTERACTIONS AT 2.7 BeV/c

Contents

Abstract v

I. Introduction 1

II. The Experiment

A. The Beam 4

B. Data Processing. 7

III. Channel Cross Sections 9

IV. The Final State $K^o\pi^+p$

A. General Features 13

B. K^* Production. 15

C. N^* Production. 29

V. The Final State $K^+p\ \pi^+\pi^-$

A. General Features 32

B. Production of K^*N^*. 35

VI. Search for Other Resonant States 49

VII. Test of SU_3 Predictions. 52

Acknowledgments. 56

Appendices

A. Symmetry of the Spin Density Matrix. 57

B. Covariant J = 3/2 Spin-Energy Projection Operator. 59

C. Derivation of Cross Section Relations

from Reaction Symmetries 61

Footnotes and References 67

K^+p INELASTIC INTERACTIONS AT 2.7 BeV/c

Riley David Newman

Lawrence Radiation Laboratory
University of California
Berkeley, California

ABSTRACT

An analysis is presented of an exposure of the Brookhaven AGS 20" hydrogen bubble chamber to a 2.65 BeV/c separated K^+ beam. Channel cross sections are presented for K^+p interactions, except those corresponding to a two prong topology. A detailed study is made of the final states $K^0p\,\pi^+$ and $K^+p\,\pi^+\pi^-$, which are dominated by the production of $K^*(891)$ and $N^*(1236)$. The reaction $K^+p \rightarrow K^*p$ is analysed in terms of a one meson exchange model modified by form factors, and results are compared with data at other energies. The model is found to give a very unsatisfactory account of the energy dependence of K^* production. The reaction $K^+p \rightarrow K^{*0}\,N^{*++}$ is analysed in terms of a pion exchange model modified to include the effects of absorption in initial and final states.

No evidence is found for production of resonant states other than $K^*(891)$, $N^*(1236)$, and ω. Relations between three body final states of K^+p reactions implied by SU_3 symmetry are derived and tested.

I. INTRODUCTION

The study of high energy particle interactions has revealed a great profusion of resonant states. It is of interest to pursue the search for new particles, and to determine their quantum numbers as they are found. It is also of great interest to ellucidate the production mechanisms for those particles whose existence and quantum numbers are well established.

A striking feature of high energy meson nucleon interactions is that they proceed in large part by way of quasi-two-body production of resonant states, and that this production tends to be strongly peaked in the forward (or backward) directions. This peaking suggests a peripheral process, and it is tempting to try a one meson exchange model (OME) for these reactions. Unfortunately, the peaking introduced in this model by the propagator for the exchanged particle is often completely masked by the momentum transfer dependence of the vertex couplings involved, and the unmodified model usually fails miserably to reproduce experimental production angular distributions and cross sections. This is not too surprising, since the model predicts an amplitude which greatly exceeds the unitary limit for low partial waves. On the other hand, resonance decay distributions are often in fair agreement with the predictions of this model.

Various modifications of the OME model have been tried to account for the observed peaking of production distributions. The first and

simplest approach was to multiply the simple OME "Born term" by a form factor--a function of momentum transfer to allow for the effects of structure in the vertices and propagator of the model. In practise this function must be determined empirically, but should not be a function of energy, so that the model may be tested by seeing if the same form factors reproduce the data at all production energies. More recently, a great deal of attention has been given to the effect on a particular production channel of competing channels. One approach to this is the absorption model, developed by Sopkovich,[1] Durand and Chiu,[2] Gottfried and Jackson,[3] and others, in which the OME amplitude is modified by the effects of absorption in the initial and final states into other channels. The greatest absorption is found in the low partial waves, as might be intuitively expected, so that the peripheral nature of the OME amplitude is enhanced, reproducing the observed forward peaking. Absorption, unlike the form factors described above, also affects the decay distributions predicted by the OME model.

The analysis of K^+p interactions is in many ways ideally suited to the study of peripheral production mechanisms. There are no resonances in the direct channel. Only two resonances are produced in significant amounts in the three and four body final states through at least 3 BeV/c--the $K^*(891)$ and $N^*(1236)$. The production of these resonances dominates these final states, so that the problem of dealing with non-resonant background is minimized. Finally, the quantum numbers of these resonances are well established, so that attention may be devoted entirely

to production mechanisms. In the sections which follow we investigate production and decay distributions for the following reactions

$$K^+p \rightarrow K^{*+}p \qquad 1a$$

$$K^oN^{*++} \qquad 1b$$

$$K^{*o}N^{*++} \qquad 1c$$

at a K^+ beam momentum of 2.65 BeV/c. Reaction 1a we will treat with an OME model modified only by form factors, comparing our results with data at other energies. Reaction 1b provides too little data for a detailed analysis. Reaction 1c we will treat with an absorption model. We then discuss the possible production of other resonances. Finally we derive and test some predictions of SU_3 symmetry relating the three body final states of K^+p reactions.

II. THE EXPERIMENT

A. The Beam

The experiment was conducted with the AGS accelerator and 20-in. bubble chamber at Brookhaven National Laboratories. The 20-in. chamber beam is shown schematically in Fig. 1 and is described in detail in the literature.[4] It consists of a transport and momentum-defining stage followed by two mass separation stages, the second of which provides additional momentum definition, and finally a beam shaping transport section to the chamber. The desired 2.7 BeV/c K^+ beam pressed the mass separation capability of the beam toward its limit. In order to achieve good mass separation care was taken to deep the vertical image and object sizes to a minimum in the beam optics. The height of the target in the AGS proton beam was .050", while the heights of slits S2, S3, and S4 in Fig. 1 were .045", .100", and .060" respectively. The πK separation achieved is indicated in a tuning curve for the second separator, shown in Fig. 2. The run was made with the indicated setting on the high side of the K peak, where allowing for some shift due to separator instability we estimate the π, μ, e contamination to be less than 10%. This estimate was confirmed by a later estimate based on a comparison of number of K^+ three prong decays observed with the number of passing tracks in the chamber. To minimize contamination from in-flight decays of K^+ in the final section of the beam, stringent acceptance criteria were imposed on the azimuthal and dip angles of beam tracks entering the bubble chamber when selecting events for analysis. The beam momentum

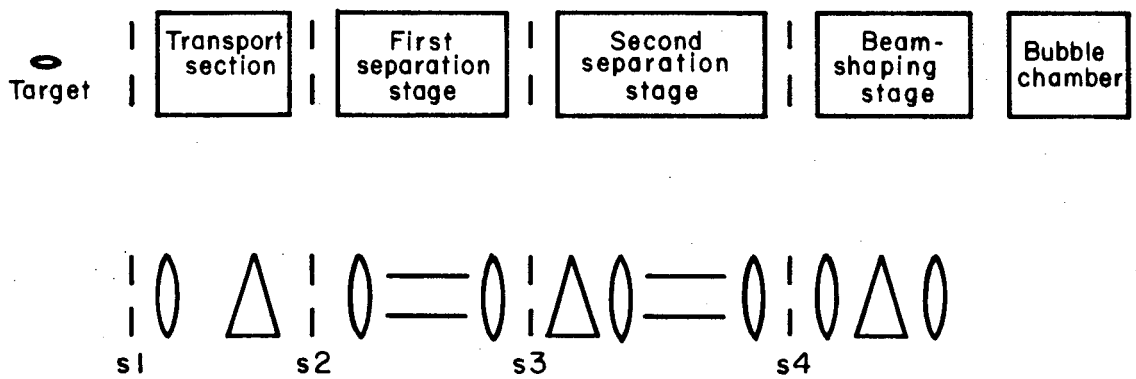

MUB-11440

Fig. 1 Schematic diagram of the beam to the Brookhaven 20" bubble chamber.

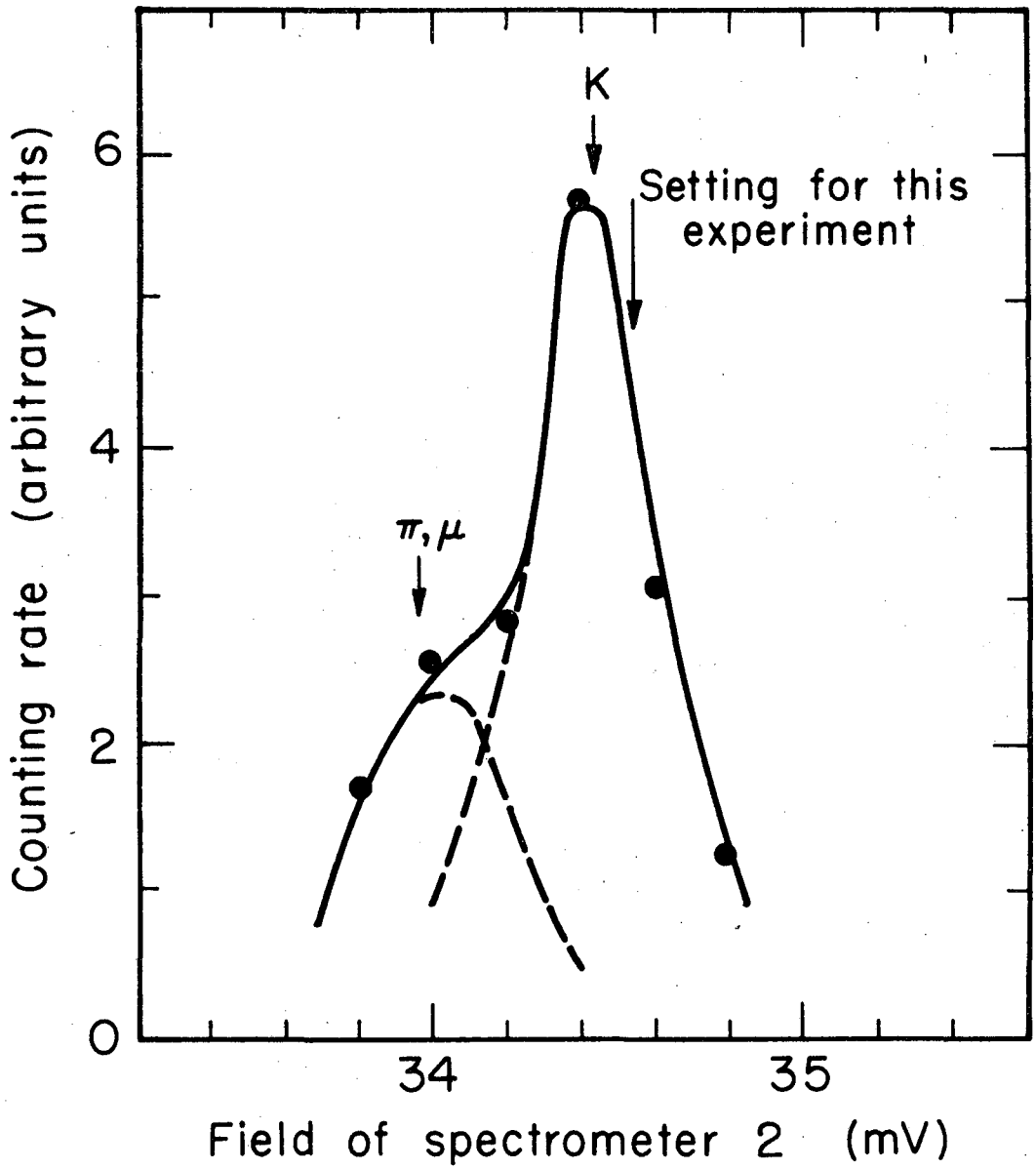

MUB-11443

Fig. 2 Beam tuning curve, indicating π-K mass separation achieved. Counting rate at the second mass separation slit (S4) is plotted vs. magnetic field in the second mass spectrometer.

was determined to be $(2.65 \pm .03)$ BeV/c from measurement of passing tracks in the chamber.

B. Data Processing

A total of 50,000 pictures was taken. All film was scanned three times to locate events, providing essentially 100% scanning efficiency. Those events having a two prong topology with no observed neutral decay were not analysed in this study. Otherwise all events were measured and processed using the PANAL-PACKAGE bubble chamber analysis computer programs.[5] For the final analysis only those events occurring in a restricted fiducial volume were accepted. For each event a kinematic fit was attempted to every known combination of strongly interacting particles consistent with the observed topology which conserved energy, strangeness, and baryon number, and which involved at most one unobserved particle. A hypothesis was accepted if two conditions were met: the χ^2 for the fit must correspond to a probability level greater than 1%, and the track bubble density observed must be consistent with the particle velocities indicated by the fit. Ambiguities were resolved on the basis of bubble density if possible, otherwise on the basis of χ^2, except in the case of the following rather common ambiguity. Among the events with four charged prongs we often find both a four constraint fit to the final state $K^+ p \pi^+ \pi^-$ and a one constraint fit to $p K^+ \pi^+ \pi^- \pi^0$. In the latter fit the π^0 is found to be nearly at rest in the laboratory frame,

and the track assignments of the K^+ and p are reversed with respect to the four constraint fit. When bubble density could resolve this ambiguity such fits were found to almost invariably "fakes". Hence when bubble density could not resolve the ambiguity the fit with π^o was rejected in favor of the four constraint fit almost regardless of relative χ^2 .

About 8% of the events yielded no acceptable fit. This is consistent with the number of events which might be expected to involve more than one unobserved neutral particle, along with those events arising from π contamination.

About 5% of the events were unmeasurable or failed in the computer processing after repeated tries. Channel cross sections derived from fitted events were scaled up accordingly.

III. CHANNEL CROSS SECTIONS

Cross sections were determined by comparing the number of events in a channel with the number of three prong events occurring in the same volume and satisfying the same beam track entrance criteria. Three prong events represent K^+ decays, providing a measure of the total K^+ track length observed. We have

$$\sigma_i = \frac{M\,\lambda(3p)}{P\,\rho}\left(\frac{N_i}{N_{3p}}\right)$$

where σ_i is the cross section for channel i, N_i is the number of events observed in channel i, N_{3p} is the number of three prong events observed in the same volume, $\lambda(3p)$ is the partial rate for K^+ decays yielding three charged prongs, P is the K^+ beam momentum, M is the mass of the K^+, and ρ is the density of the bubble chamber hydrogen, in protons/cm^3. To determine $\lambda(3p)$ we consider the K^+ decay modes yielding three charged particles:

Mode		Branching Ratio[6]	
$\pi^+\ \pi^o$	$\pi^o \to e^+\ e^-\ \gamma$	.216 ± .006	× .0119 ± .0005
$\pi^o\ \mu^+\ \nu$		.032 ± .004	
$\pi^o\ e^+\ \nu$		.045 ± .003	
$\pi^+\ \pi^o\ \pi^o$		.017 ± .001 x 2 x .0119	
$\pi^+\ \pi^+\ \pi^-$		.056 ± .001	
	Total	.060 ± .001	

Dividing by the K^+ lifetime $\tau_{K^+} = 1.243 \pm .004\ 10^{-8}$ we get a three prong partial rate: $\lambda(3p) = 4.83 \cdot 10^6 \pm 1.6\%$.

The hydrogen density ρ was determined from the hydrogen temperature T, which in turn was determined from a neon vapor pressure thermometer in the chamber, monitored during the run. The values found were: $T = 26.0 \pm .1\ ^oK$, $\rho = .0626 \pm .0003\ gm/cm^3 = 3.74\ 10^{22}$ protons/cm^3.

With a few exceptions, information on final states including a K^o or Λ was derived only from those events in which the K^o or Λ was observed to decay within a preset volume in the chamber. To obtain cross sections, the number of such events requires two corrections. The first is a factor of 2.89 for K^o events[6] and 1.5 for Λ events, to take into account the K_2 and neutral decay modes of these particles. The second is an escape correction to allow for those K_1 or Λ which decay outside the acceptance volume. This correction was made by weighting each event with a factor $w_i = (1-P_i)^{-1}$ where P_i is the probability, for that event, that the K^o or Λ would reach the boundary of the acceptance volume without decaying. This is given by $P = \exp(-t/T)$, where T is the mean lifetime of the particle and t is the proper time it would have spent on its path from production to boundary of acceptance volume, had it not decayed. The average value of the factor w was about 1.2 for K^o decays, and 1.3 for Λ decays.

Cross section data for all channels accessible to this study are presented in Table 1. Parentheses around a neutral particle indicate its decay is not observed. Errors are statistical, based on the number

of events observed in each channel combined with a statistical uncertainty of 8% in the number of three prong events used to determine cross sections. Errors in the remaining quantities entering the cross section determination -- $\lambda(3p)$, beam momentum, and hydrogen density--are negligible in comparison to these factors.

Table I. Cross sections for K^+p inelastic reactions at 2.65 BeV/c

Channel	Cross section (mb)
$K^o p\pi^+$	2.7 ± 0.3
$K^o p\pi^+(\pi^o)$	1.9 ± 0.2
$K^o\pi^+\pi^+(n)$	0.64 ± 0.12
$K^+p\pi^+\pi^-$	2.6 ± 0.2
$K^+p\pi^+\pi^-(\pi^o)$	0.43 ± 0.06
$K^+\pi^+\pi^+\pi^-(n)$	0.14 ± 0.03
$p\pi^+\pi^+\pi^-(K^o)$	0.14 ± 0.03
$p\pi^+\pi^+\pi^-K^o(\pi^o)$	0.04 ± 0.04
$K^+p\pi^+\pi^+\pi^-\pi^-$	0.01 ± 0.01
$K^+K^o\Sigma^+$	0.02 ± 0.02
$K^+K^+\Sigma^o$	$\lesssim$.01
$K^+K^+\Lambda$	0.03 ± 0.02
$K^+K^+\Lambda(\pi^o)$	0.01 ± 0.01
$K^oK^+\pi^+(\Lambda)$	0.03 ± 0.03

IV. The Final State $K^o \pi^+ p$

A. General Features

The final state $K^o \pi^+ p$ with observed K^o decay may be identified with virtually no ambiguities. The effect of π contamination is negligible; the $\pi^+ p$ final states which might be mistaken for this one are $\bar{K}^o K^+ p$, $\bar{K}^o K^+ p \pi^o$, $K^o \bar{K}^o p \pi^+$, and $n K^+ \pi^+ \bar{K}^o$, with a combined cross section at this energy of only .068 mb,[7] and these are easily distinguishable kinematically.

A Dalitz plot of the $K^o \pi^+ p$ events is shown in Fig. 3, along with projections onto the $m^2(K \pi)$ and $m^2(p \pi)$ axes. Clearly this state is dominated by the production of $K^*(891)$ and $N^*(1236)$. To estimate the relative amount of K^* and N^* in this state a maximum likelihood fit was made to the Dalitz plot distribution assuming a sum of non-interfering contributions from uniform background, $K^* p$, and $N^* K^o$ production:

$$f(\vec{a}\ ;\ m^2_{k\pi}\ ,\ m^2_{p\pi}) = a_1\ f_B + a_2\ f_{K^*}(m_{k\pi}) + a_3\ f_{N^*}(m_{p\pi})$$

where $\vec{a}$ gives the relative amounts of the three contributions, constrained by $a_1 + a_2 + a_3 = 1$, and each f_i is normalized to one over the Dalitz plot. f_B is a constant, while f_{K^*} and f_{N^*} were taken to be of the form:

$$N \frac{\frac{m}{p}\ \Gamma(m)}{(m^2 - m^{*2})^2 + m^{*2}\ \Gamma^2(m)} \quad .$$

Here letting a and b denote the products of the resonance decay, m is

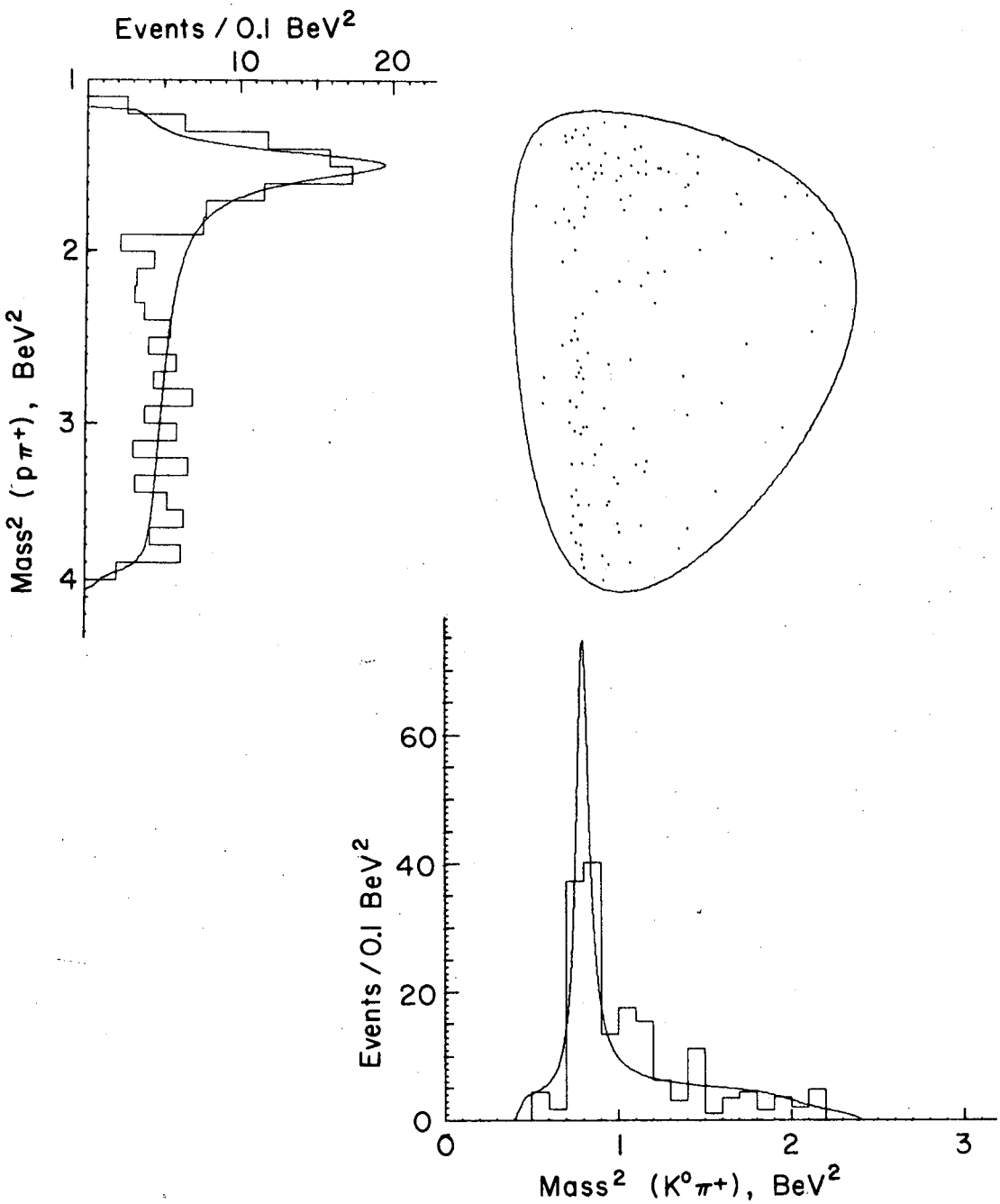

MUB-11445

Fig. 3 Dalitz plot for the final state $K^{o}p\pi^{+}$. Events in the mass histogram are weighted as described in the text. Curves plotted on the histograms correspond to the production of $K^{*}(891)$, $N^{*}(1236)$, and non-resonant background in proportions determined from a likelihood fit to the Dalitz plot distribution.

the effective mass of the pair ab , p is the rest frame momentum for the decay $m \to a + b$, m^* is the resonant mass, $\Gamma(m)$ is an energy dependent decay width normalized so that $\Gamma(m^*)$ is the resonance width, and N normalizes the distribution to one over the Dalitz plot. The factor m/p removes the phase space dependence from the Γ in the numerator. We take $\Gamma(m)$ proportional to $\frac{p^3}{m^2}$ for the K^* and proportional to $\frac{p^3}{m}(E_b + m_b)$ for the N^* , where m_b and E_b are the mass and energy respectively of the proton in the N^* rest frame. Masses and widths of the resonances were input to the fit:

$$m_{K^*} = 891,\ m_{N^*} = 1236,\ \Gamma_{K^*} = 50,\ \Gamma_{N^*} = 120 .$$

In making the fit each event was weighted with the escape correction factor w_i defined in Section III, so that the likelihood function becomes:

$$\mathcal{L}(\vec{a}) = \prod_i f(\vec{a};\ x_i)^{w_i}$$

where x is the position on the Dalitz plot. Statistical errors however were estimated from a likelihood function calculated without weights. The fit indicates (12 ± 8)% background, (56 ± 7)% K^*p and (32 ± 7)% N^*K^0 . Curves corresponding to these values are plotted on the weighted $m^2(K\pi)$ and $m^2(p\pi)$ distributions in Fig. 3. The corresponding K^* and N^* production cross sections in this channel are 1.5 ± .3 mb. and .9 ± .2 mb. respectively.

B. <u>K^* Production</u>

For the analysis of K^* production we select events lying in a

K^* band: $.850 < m_{K\pi} < .930$, but not in an N^* band: $1.16 < m_{p\pi} < 1.30$. By integrating the distributions $a_i f_i$ described in the last section we estimate our sample to be 94% K^*p , 3% N^*K , and 3% background.

The decay distribution of the K^* is given in terms of its spin density matrix elements by

$$w(\theta,\varphi) = \frac{3}{4\pi}\left[\rho_{00}\cos^2\theta + \rho_{11}\sin^2\theta - \rho_{1-1}\sin^2\theta\cos 2\varphi - \sqrt{2}\,\mathrm{Re}\rho_{10}\sin 2\theta\cos\varphi\right] \tag{1}$$

with $\rho_{00} = 1-2\rho_{11}$. A discussion of the symmetry of ρ is given in Appendix A. Here θ and φ are polar angles in a coordinate system in which the y axis is taken to be normal to the production plane. If the z axis is taken to be the direction of the incident K^+ in the K^* rest frame, ρ_{00} may be interpreted as the relative contribution of pseudoscalar exchange in the framework of a one meson exchange model involving the exchange of vector and pseudoscalar particles. This interpretation is not affected if the exchange process is modified by form factors. The value of ρ_{00} will be altered if absorption effects are important, but still may be expected to give an indication of the relative importance of pseudoscalar exchange.

The parameters ρ_{00} , ρ_{1-1} and $\mathrm{Re}\rho_{10}$ were evaluated from a single maximum likelihood fit to the K^* decay distribution.[8] In making this fit each event was weighted with its escape correction factor, as in the fit to the Dalitz plot distribution. To avoid biases arising from the omission of the part of the K^* band which overlaps the N^* band, we exploit the fact that distribution 1 is invariant under the transfor-

mation $\theta \to \pi - \theta$, $\varphi \to \varphi + \pi$. The overlap is so located that if an event lies in the overlap region, then its "conjugate" event lies outside it. In making the fit each event was given a weight factor of two if its "conjugate" lies in the overlap region, thus effectively "replacing" the excluded events. In Table II we present the density matrix parameters determined for the total K^* sample. Results are given both for an unweighted fit and for a fit weighted as described above. The two fits agree within the errors.

Table II. K^* Spin density matrix elements for the channel $K^{*+}p$

Parameter	Unweighted fit	Weighted fit
ρ_{00}	0.16 ± 0.08	0.20 ± 0.08
$\rho_{1,-1}$	0.23 ± 0.09	0.19 ± 0.09
$\mathrm{Re}\rho_{10}$	-0.13 ± 0.03	-0.16 ± 0.03

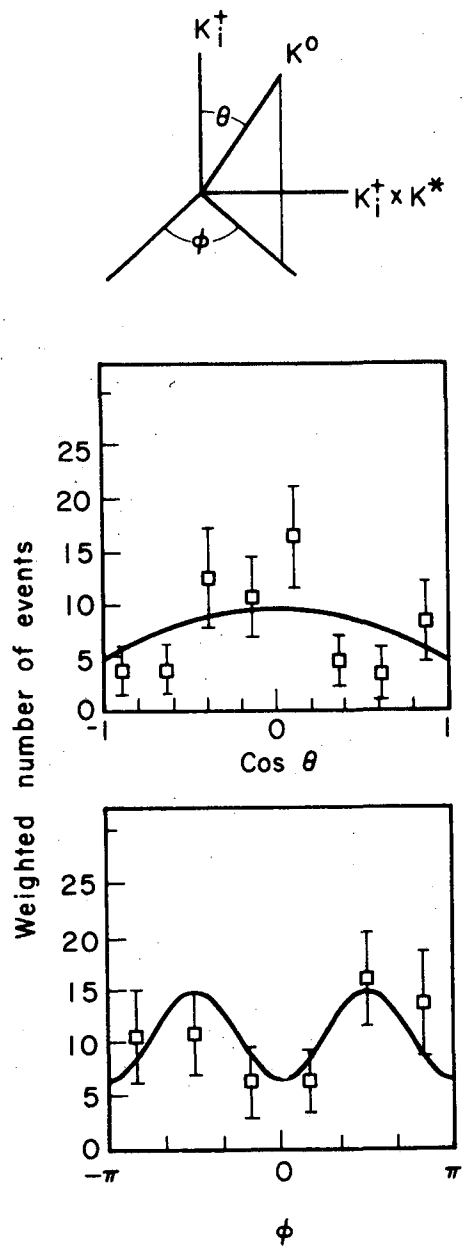

MUB-11405

Fig. 4 Decay angular distributions for the K^* in the channel $K^{*+}p$. Particle symbols in the coordinate system diagram represent the direction of motion of the particles in the K^* rest frame. Events are weighted as described in the text. Curves are determined by K^* density matrix parameters obtained from a three parameter likelihood fit to the (θ,φ) distribution.

An alternative method for determining $\mathrm{Re}\rho_{10}$ which is often used is to evaluate $\mathrm{Re}\rho_{10} = \frac{-5}{4\sqrt{2}} < \sin 2\theta \cos\varphi >$. For our unweighted data this method yields $\rho_{10} = -0.17$, in reasonable agreement with the result of our likelihood fit. In Fig. 4 we show the weighted decay distributions in $\cos\theta$ and φ for the total K^* sample, along with the curves determined by distribution 1 using our results for ρ_{00} and ρ_{1-1} . Note that distribution 1 averaged over φ gives a distribution in $\cos\theta$ which depends only on ρ_{00} , while averaged over $\cos\theta$ it gives a distribution in φ depending only on ρ_{1-1} . However the values of ρ_{00} and ρ_{1-1} are coupled to the value of $\mathrm{Re}\rho_{10}$ in making our likelihood fit. Hence the curves plotted in Fig. 4 are not necessarily the best possible fit to the corresponding histograms, but reflect additional information on θ-φ correlations. The same comment applies to all K^* and N^* decay distributions discussed in this study.

We now approach our data with a one meson exchange model modified by form factors, following the approach of Jackson and Pilkuhn.[9] We first ask what particles may be exchanged. Restricting the possibilities to low mass particles allows the exchange of η , π , ρ , ω and φ mesons. Evidence against the importance of ρ exchange is provided by results of a study[10] of the reaction $K^+n \rightarrow K^{*o}p$, in which the exchange of an isoscalar meson is forbidden. The exchange of either π or ρ is allowed in that reaction, but in fact the contribution of vector exchange is very small, indicating that ρ exchange does not

contribute significantly. Isospin invariance of the vertices then extends that conclusion to our reaction. The absence of ρ exchange provides some support for the conservation of A parity,[11] which forbids a $\rho K K^*$ coupling. Conservation of A parity would also forbid a $\varphi K K^*$ coupling. This, along with the high mass of the φ, provides arguments against the importance of φ exchange in our reaction. As for the η, SU_3 symmetry using a D/F ratio of 2.0 indicates $g^2_{pp\eta}/g^2_{pp\pi^o} = \frac{1}{27}$, while at the meson vertex we have $g^2_{KK^*\eta}/g^2_{KK^+\pi^o} = 3$. This, along with the high mass of the η compared to the π^o, indicates that the contribution of η exchange to our reaction will be small compared to π exchange. Hence we restrict our model to the exchange of π and ω mesons.

Treating the K^* as a stable particle, we may write its production cross section with the one meson exchange model (OME) as[9]

$$\frac{d\sigma}{d\Omega} = \frac{d\sigma_p}{d\Omega} + \frac{d\sigma_v}{d\Omega}$$

where, with a factor for the $K^* \to K^o\pi^+$ branching ratio,

$$\frac{d\sigma_p}{d\Omega} = \frac{2q'}{3sq} \frac{g^2}{4\pi} \frac{G^2}{4\pi} \Delta^2 a_c^2 \left| \frac{F_p(\Delta^2)}{m_\pi^2+\Delta^2} \right|^2$$

is the contribution from π exchange, and

$$\frac{d\sigma_v}{d\Omega} = \frac{q'}{3sq} \frac{f^2}{4\pi} \left| \frac{F_v(\Delta^2)}{M_v^2+\Delta^2} \right|^2 \left[\frac{(G_v+G_T)^2}{4\pi} \Delta^2 a_c^2 + \frac{2\, s\, q^2\, q'^2 \sin^2\theta}{M_{K^*}^2} \left(\frac{G_v^2}{4\pi} + \frac{G_T^2}{4\pi} \frac{\Delta^2}{4M_p^2} \right) \right]$$

is the contribution from vector meson exchange. Here a_c is the momentum of the incident K^+ in the rest frame of the K^*, given by

$$a_c^{\,2} = \frac{1}{4M_{K^*}^2}\left[\Delta^2 + (M_K - M_{K^*})^2\right]\left[\Delta^2 + (M_K + M_{K^*})^2\right]$$

s is the square of the C.M. energy, q is the C.M. momentum of the K^+, q' is the C.M. momentum of the K^*, and Δ^2 is the momentum transfer to the K^*. In the π exchange contribution $\frac{g^2}{4\pi}$ is the $K^+ \pi^o K^{*+}$ coupling constant, estimated from the K^* decay width to be about .75, $\frac{G^2}{4\pi} \approx 15$ is the $NN\pi^o$ coupling constant, and $F_p(\Delta^2)$ is a form factor. In the vector exchange contribution $\frac{f^2}{4\pi}$ is the vector meson coupling constant at the $K K^*$ vertex, G_V and G_T are coupling constants at the nucleon vertex, and $F_v(\Delta^2)$ is a form factor. Of the vector coupling constants little is known, except that one can argue[9] for ω exchange that $G_T \approx 0$. The unknowns then in these expressions are the product $f^2 G_V^{\,2}$ and the two form factors $F_p(\Delta^2)$ and $F_v(\Delta^2)$.

For K^* production at 3.0 BeV/c [12] the contribution of pseudoscalar exchange was found to be very small, and a good fit to the data was obtained assuming ω exchange alone, with $\frac{f^2}{4\pi}\frac{G_V^{\,2}}{4\pi} = 12$, $F_v(\Delta^2) = \exp\left[-\Delta^2/(.7\ \text{BeV/c})^2\right]$, and $M_v = .750$ BeV. Using the above form factor and coupling constants an attempt has been made to fit K^* production cross sections at 1.96 BeV/c.[13] At that energy the contribution of π exchange is considerable, and the measured value of ρ_{00} was used to estimate σ_p and σ_v. The observed value of

σ_v was a factor of two greater than predicted using the parameters from the 3 BeV/c data. On the other hand, σ_p was predicted quite well using the known coupling constants along with a form factor

$$F_p(\Delta^2) = \frac{\alpha^2 - m_\pi^2}{\alpha^2 + \Delta^2} \quad \text{with} \quad \alpha^2 = .165(\text{BeV/c})^2 \quad .$$

This form factor had given reasonable fits at 1.96 and 3.0 GeV/c to the reaction $K^+p \rightarrow K^*N^*$, which has been found to proceed mainly by pion exchange.[14,15]

We are now prepared to apply the model to our experiment, and to make further comparisons with data at other energies. To do so, we adopt the pion and vector exchange form factors defined above and take $M_v = .783$. For the product $\frac{f^2}{4\pi}\frac{G_v^2}{4\pi}$ we try two values, 13.4 and 28.6, which when the pion exchange contribution is included reproduce the observed total K^*p production cross section at 3.0 and 2.65 BeV/c respectively. The tests of the model will be 1) the shape of the K^* production angular distribution at our energy, 2) the energy dependence of the K^* production cross section, and 3) the relative contribution of pseudoscalar and vector exchange as a function of production energy.

Our K^* production distribution, weighted with K^o escape corrections, is presented in Fig. 5. Curves a and b are the OME predictions using the vector coupling value of 13.4 and 28.6 respectively. Except for a curious bump in the backward direction, the curves reproduce the shape of the experimental distribution reasonably

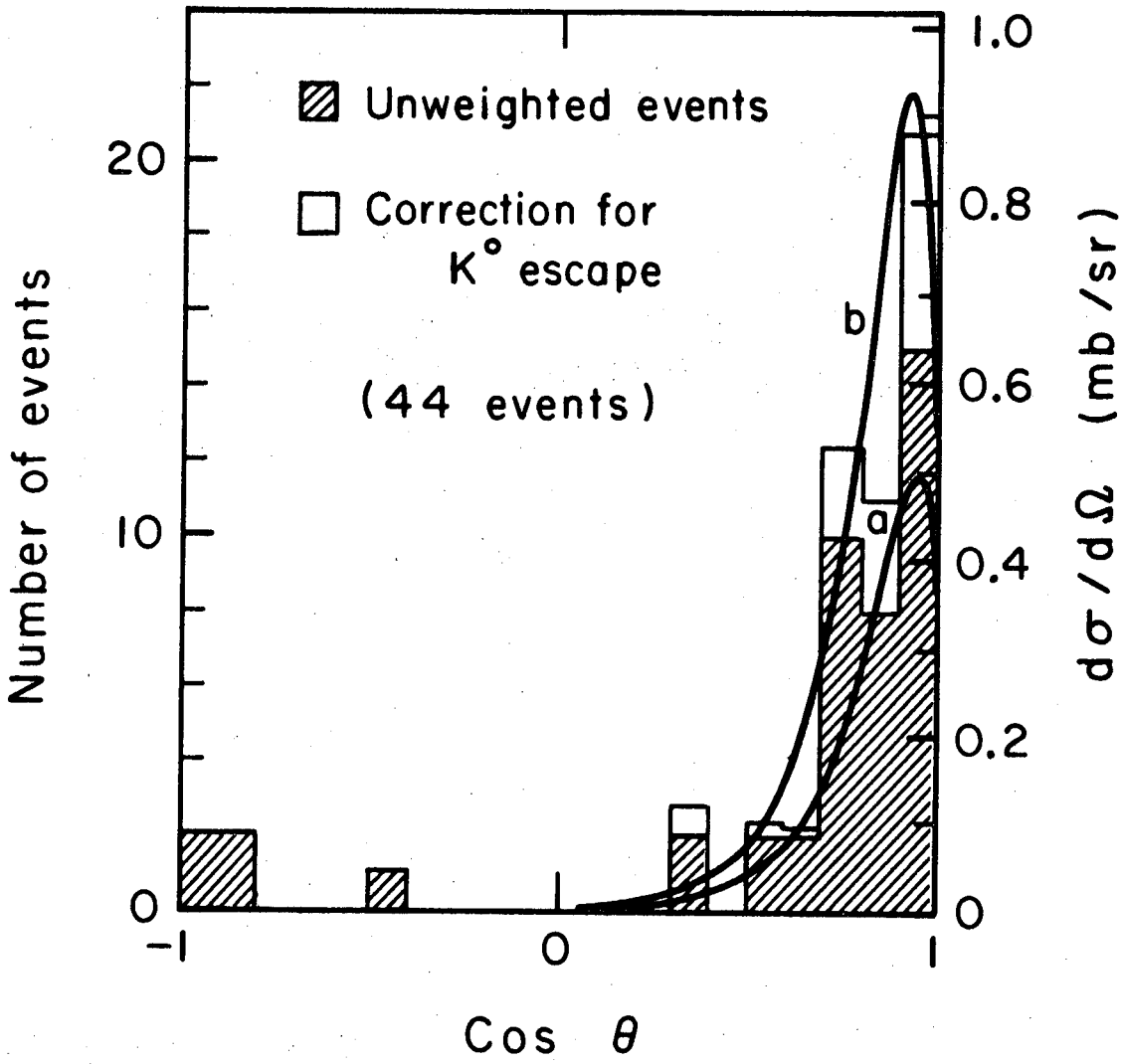

MUB-11563

Fig. 5 K^* production angular distribution for the reaction $K^+p \rightarrow K^{*+}p$. The curves are predictions of a one meson exchange model modified by form factors, with π and ω exchange. Values of the vector coupling constant $f^2G_V^2$ are chosen to reproduce the $K^{*+}p$ total cross section at 3.0 BeV/c (curve a) and 2.65 BeV/c (curve b).

well, considering the limited statistics. In magnitude, curve a, which represents an extension of the expression fitting 3.0 BeV/c data, is much too small. Curve b agrees in magnitude by construction.

Total $K^+p \rightarrow K^*p$ cross sections from a number of experiments are plotted as a function of production beam momentum in Fig. 6. Curves a and b have the same meaning as before. Curves c and d are respectively the π and ω exchange contributions to curve a. Here we see very dramatically the failure of the simple OME model to reproduce the energy dependence of the K^* production cross section. The predicted cross section rises steadily, while experimentally it rises steeply at threshold and then falls off rapidly. This experimental behavior corresponds closely to that of the total cross section for the channel $K^o\pi^+p$, which is shown in Fig. 7. The falling off of this cross section becomes understandable when we note that the total K^+p cross section above K^* threshold is nearly constant, so that the opening up of new multibody channels is necessarily at the expense of the $K^o\pi^+p$ cross section, and hence of the K^*p cross section. Thus it becomes dramatically clear that a model for K^*p production must take into account the effect of competing channels.

From Fig. 6 we see that the rise of the OME cross section with energy results from the vector exchange contribution. This increase with energy is a well known difficulty associated with vector exchange models. As we see here, this behavior is not controlled by the addition

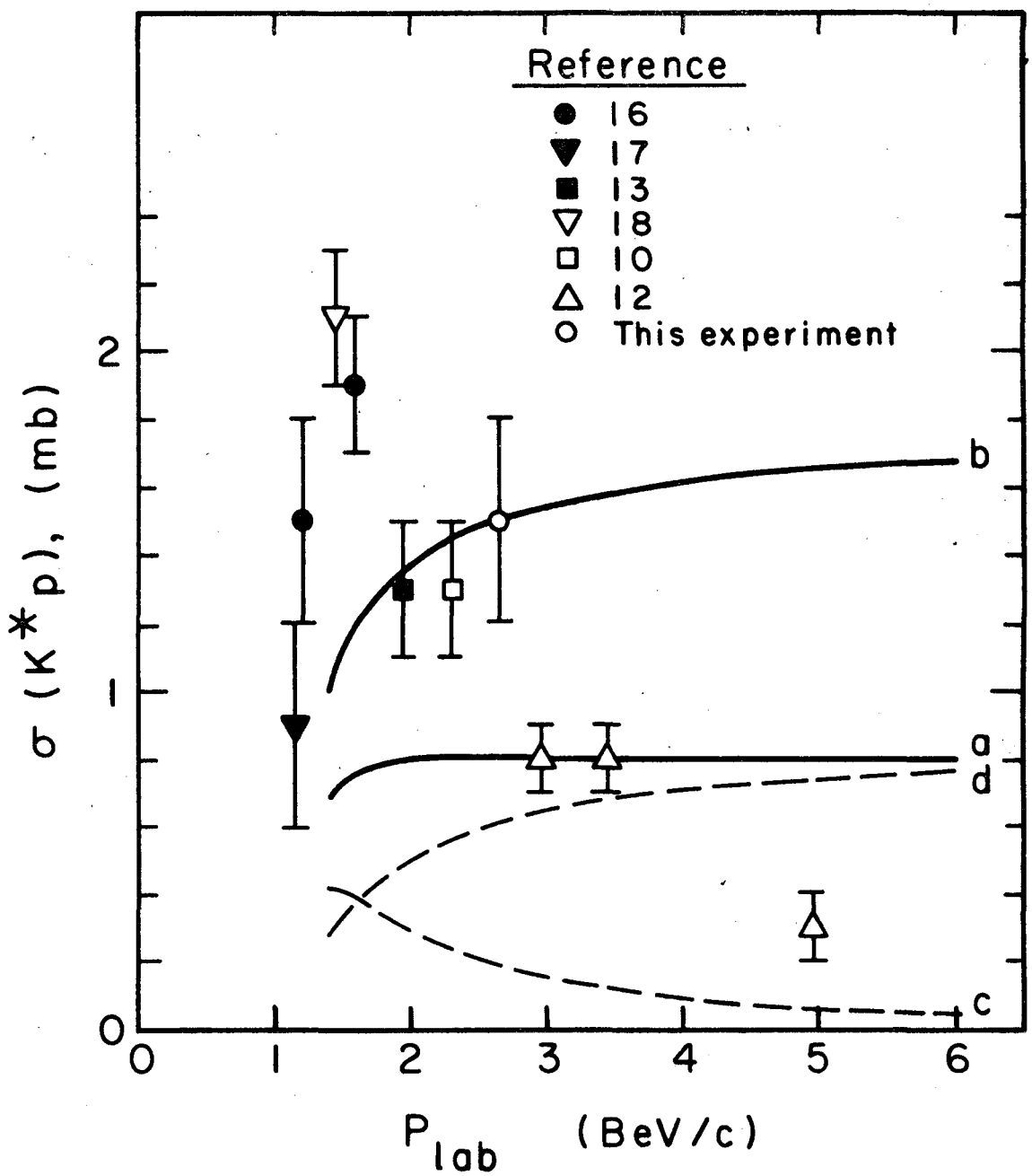

MUB 11564

Fig. 6 Energy dependence of the cross section for the reaction $K^+p \rightarrow K^{*+}p$, $K^{*+} \rightarrow K^0\pi^+$. Curves a and b have the same meaning as in Fig. 5, while curves c and d represent the π and ω exchange contributions to curve a .

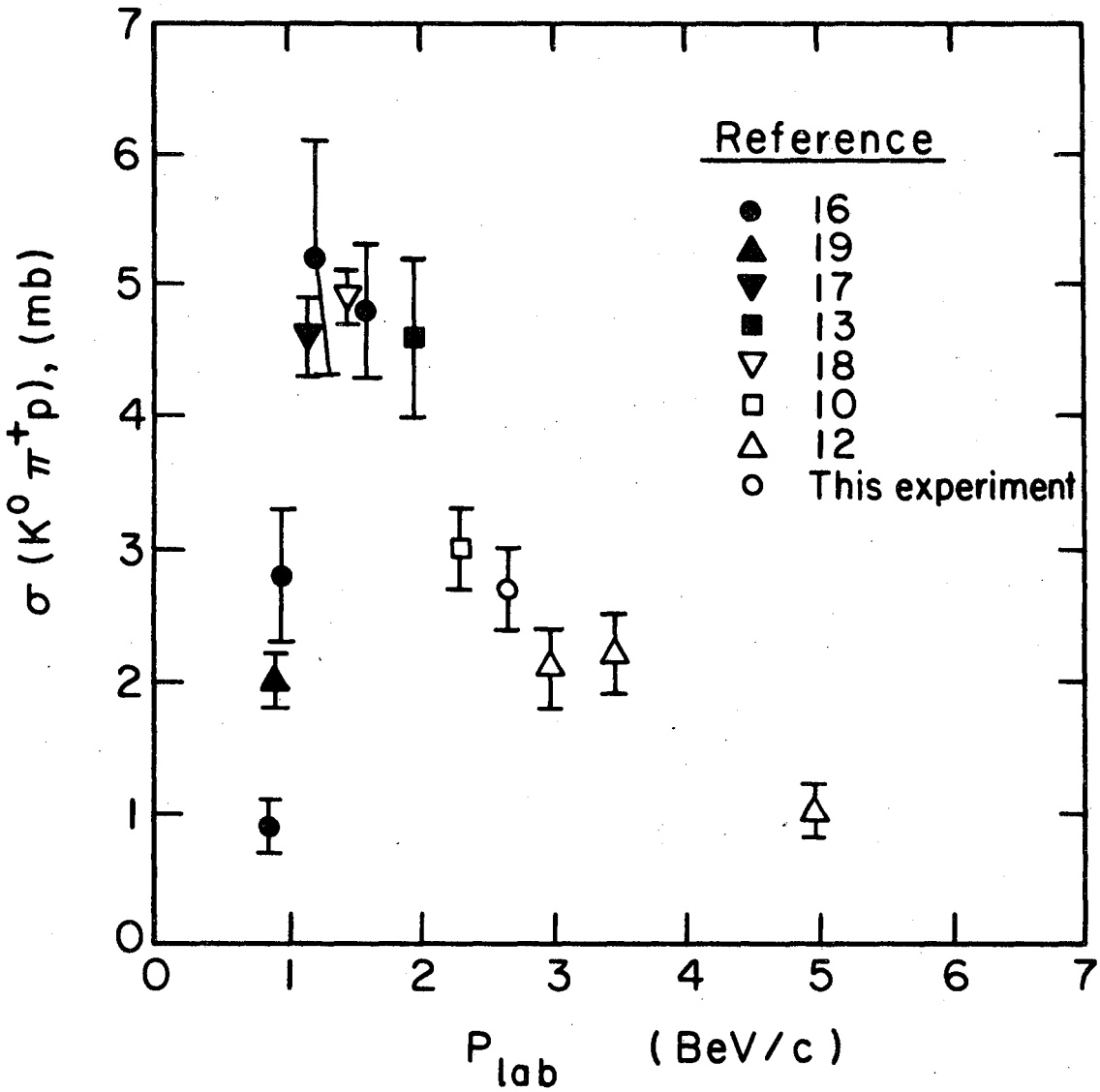

MUB-11565

Fig. 7 Energy dependence of the cross section for the reaction $K^+p \rightarrow K^o\pi^+p$.

of a form factor. Unfortunately, it is also not tamed satisfactorily by the absorption model as formulated by Jackson and others.[23,24]

Next we compare in Fig. 8 the observed values of the density matrix parameter ρ_{00} at several production momenta with the predictions of the model. The values of ρ_{00} are averaged over momentum transfer, and as indicated earlier give a measure of the relative importance of pseudoscalar exchange. Curves a and b have the same meaning as before. Here the simple OME model gives a somewhat more accurate prediction.

Finally we note that the OME model used above implies a zero value of the density matrix parameter $\mathrm{Re}\rho_{10}$, although inclusion of absorption effects predicts in general a nonzero value. In fact we find that parameter to be $-.16 \pm .03$, indicating another failure of the simple model we have applied.

In conclusion we note that the OME model modified only by form factors gives rather poor agreement with the data on the reaction $K^+p \to K^*p$. Production angular distributions are reproduced only by fitting with drastic form factors of rather arbitrary form, while the energy dependence of the reaction cross section is reproduced very badly. It is not likely that the inclusion of η or φ exchange contributions could alter this conclusion.

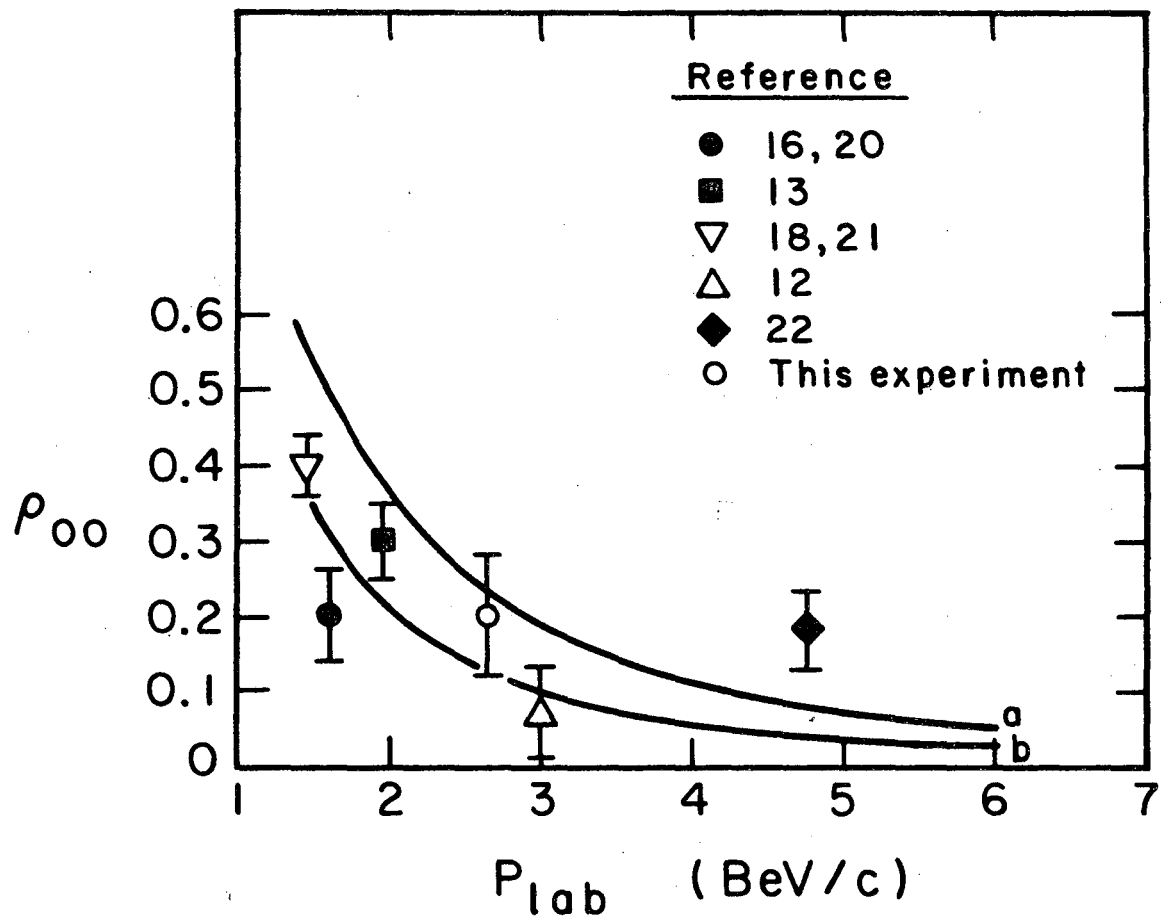

MUB 11566

Fig. 8 Energy dependence of the K^* density matrix element ρ_{00} in the reaction $K^+p \rightarrow K^{*+}p$. Curves a and b have the same meaning as in Fig. 5.

C. N^* Production

For our analysis of $N^*(1236)$ production we select events lying in an N^* band but not in a K^* band, with the bands as defined in Section B. The production angular distribution for these N^* events is presented in Fig. 9. Like the K^* distribution, it is strongly peaked at low momentum transfers. Because of the limited number of events, we have made no comparisons with models for N^* production.

The decay distribution of the N^* is given in terms of the elements of its spin density matrix by

$$w(\theta,\varphi) = \frac{3}{4\pi}\left[\rho_{33} \sin^2\theta + (\tfrac{1}{2} - \rho_{33})(\tfrac{1}{3} + \cos^2\theta) - \frac{2}{\sqrt{3}} \mathrm{Re}\rho_{3,-1} \sin^2\theta \cos 2\varphi - \frac{2}{\sqrt{3}} \mathrm{Re}\rho_{31} \sin 2\theta \cos\varphi \right] \qquad (2)$$

where the y axis is taken to be the normal to the production plane. Using the coordinate system[8] defined in Fig. 9, we have determined the parameters ρ_{33}, $\mathrm{Re}\rho_{3,-1}$ and $\mathrm{Re}\rho_{31}$ by making a single maximum likelihood fit to the decay distribution for our sample. Corrections for K^o escape and for omission of the overlap of the K^* and N^* bands were made in the same way as in fitting the K^* decay distribution, described in the preceding section. In Table III we present the N^* density matrix parameters determined from a fit with and without these corrections. Evaluating $\mathrm{Re}\rho_{31} = \frac{-5\sqrt{3}}{8} < \sin 2\theta \cos\varphi >$ gives a value $\mathrm{Re}\rho_{31} = 0.07$, in reasonable agreement with the result of the likelihood fit. In Fig. 9 we show the weighted decay distributions in $\cos\theta$

and φ for the N^* sample, along with curves determined by distribution 2 using our results for ρ_{33} and $\rho_{3,-1}$.

Table III. N^* Spin density matrix elements for the channel $N^{*++} K^0$

Parameter	Unweighted fit	Weighted fit
ρ_{33}	0.50 ± 0.10	0.50 ± 0.10
Re $\rho_{3,-1}$	0.17 ± 0.07	0.19 ± 0.07
Re ρ_{31}	0.11 ± 0.06	0.09 ± 0.07

It is interesting to note that the number of "conjugate" events used to replace the N^* events in the overlap region of the K^* and N^* bands, plus the corresponding number of events for the K^* sample, is seven--exactly the number of events which actually lie in the overlap region for our sample. The number of events predicted by integrating the distribution of our fit over the overlap region is 8. Thus there is apparently neither constructive nor destructive interference between K^* and N^* amplitudes in the overlap region.

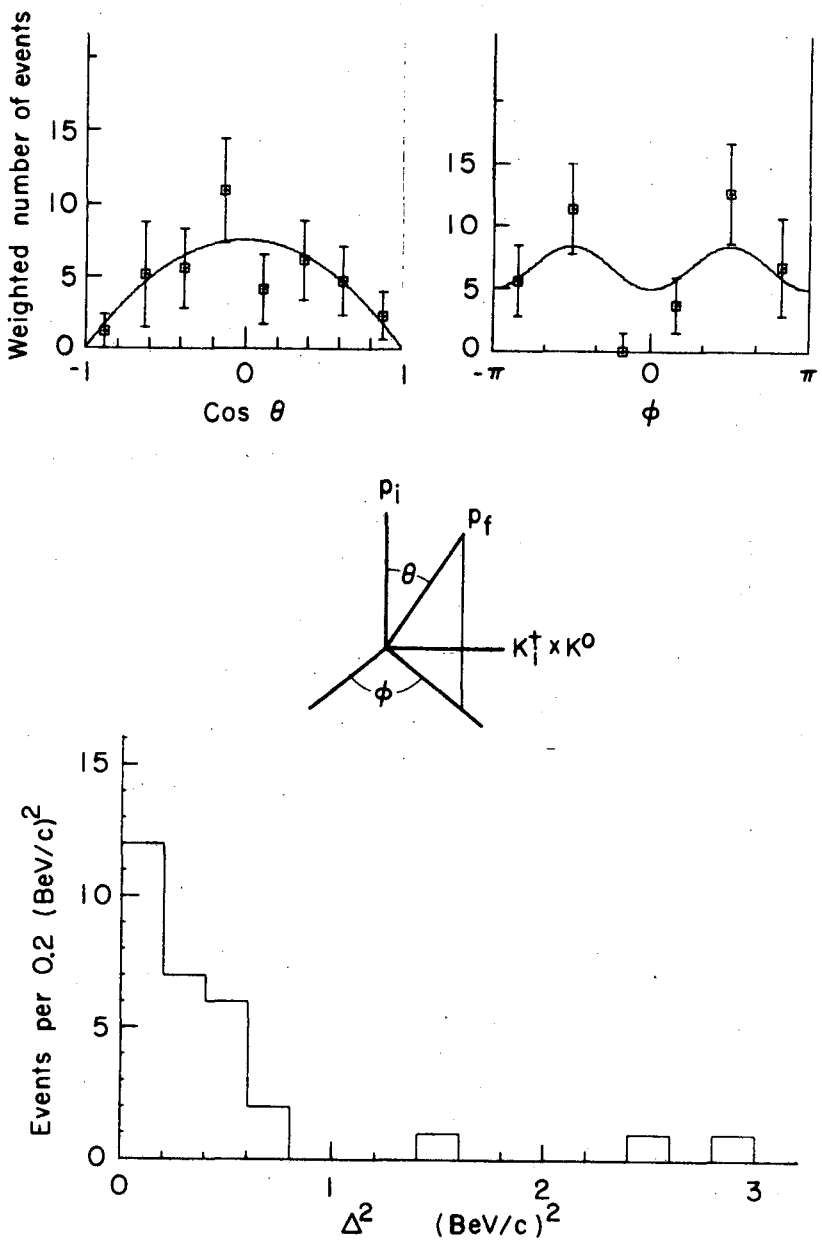

MUB-11404

Fig. 9 Production and decay distributions for the N^* in the channel $N^{*++}K^0$. Particle symbols in the coordinate system diagram represent the direction of motion of the particles in the N^* rest frame. Events in the decay distributions are weighted as described in the text. Curves are determined by N^* density matrix parameters obtained from a fit to the (θ,φ) distribution.

V. THE FINAL STATE $K^+p\ \pi^+\pi^-$

A. General Features

We first consider the effect of pion contamination in the beam on our sample of the final state $K^+p\ \pi^+\pi^-$. The reactions

$$K^+p \rightarrow K^+p\ \pi^+\pi^- \qquad (1)$$

and

$$\pi^+p \rightarrow \pi^+p\ \pi^+\pi^- \qquad (2)$$

are indistinguishable if one of the final state π^+ in reaction 2 has a momentum comparable to the beam momentum. About 25% of our events of type 1 also fit reaction 2. We may estimate that about twice as large a fraction of true events of type 2 also fit reaction 1, since it is sufficient for either of the two π^+ in reaction 2 have a large momentum in order to fake reaction 1. The cross section for reaction 1 at our beam momentum is 2.6 mb, uncorrected for pion contamination. For the second reaction the cross section is 3.5 mb.[25] Thus we must estimate that the fraction of events in our sample of reaction 1 which actually represent reaction 2 is approximately .7 times the fraction of pion contamination in our beam, which we have estimated to be $<10\%$.

In Fig. 10 we present for the channel $K^+p\ \pi^+\pi^-$, a "triangle" scatter plot of the $K^+\pi^-$ and $p\pi^+$ effective masses. It is clear that this channel is dominated by the production of $K^*(891)$ and $N^*(1236)$. To estimate the amount of this production we have made a maximum likelihood fit to the distribution of the "triangle" plot assuming non-interfering contributions from the production of K^* and N^* together, of K^* alone, of N^* alone, and of non-resonant

background. The assumed distribution is

$$F(\vec{a};m_{K\pi^-},m_{p\pi^+}) = \left[a_1 N_1 f_{K^*}(m_{K\pi^-}) f_{N^*}(m_{p\pi^+}) + a_2 N_2 f_{K^*}(m_{K\pi^-}) + a_3 N_3 f_{N^*}(m_{p\pi^+}) + a_4 N_4 \right] \frac{p q_1 q_2}{W} \quad . \tag{3}$$

Here $m_{K\pi^-}$ and $m_{p\pi^+}$ are the effective masses of the particle pairs $K^+\pi^-$ and $p\pi^+$ respectively, and the four coefficients a_i give the relative contributions of the processes listed above, with $\sum_i a_i = 1$.

The factor $\frac{p q_1 q_2}{W}$ gives the phase space associated with a position on the triangle plot, where p is the C.M. momentum of the $p\pi^+$ system, q_1 is the momentum of the π^+ in the $p\pi^+$ rest system, q_2 is the momentum of the π^- in the $K\pi^-$ rest system, and W is the C.M. energy of the reaction. The functions f_{K^*} and f_{N^*} are the same as those defined in the preceding section. The normalization constants N_i are chosen so that the integral of F over the triangle plot is one for all values of the a_i .

The result of the fit indicates the following percentages

$K^+p \rightarrow K^{*o} N^{*++}$	$(53 \pm 4)\%$
$K^{*o} p\pi^+$	$(9 \pm 4)\%$
$N^{*++} K^+\pi^-$	$(19 \pm 4)\%$
$K^+p\ \pi^+\pi^-$ (non-resonant)	$(19 \pm 4)\%$

Curves corresponding to this combination of resonance production are plotted on the projections of the scatter plot in Fig. 10.

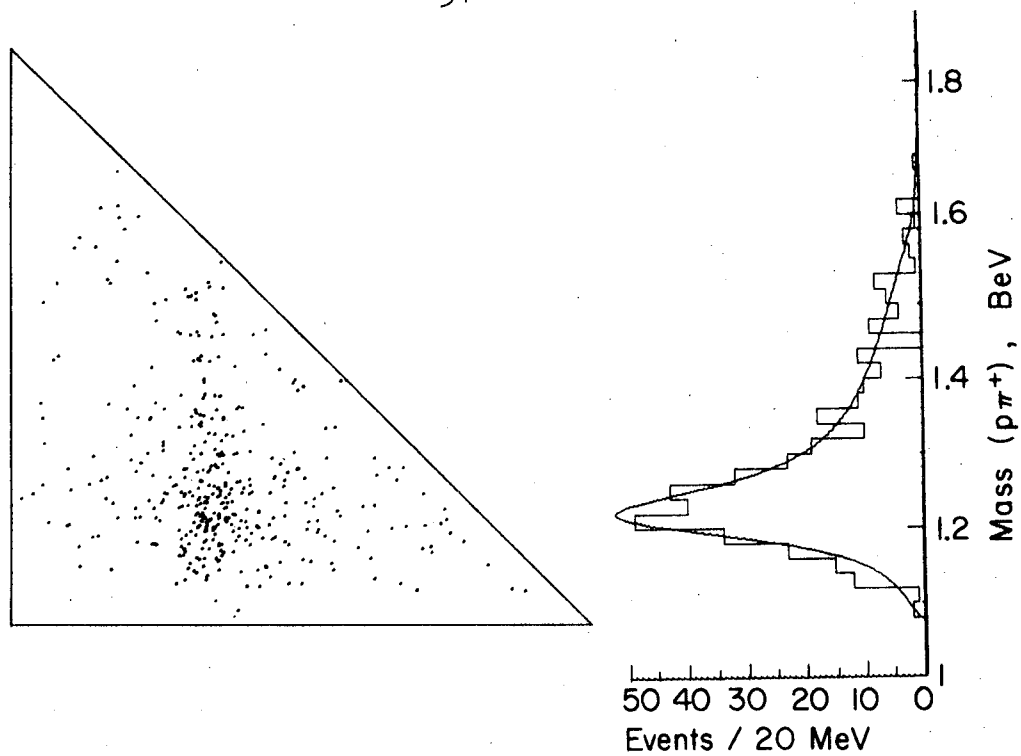

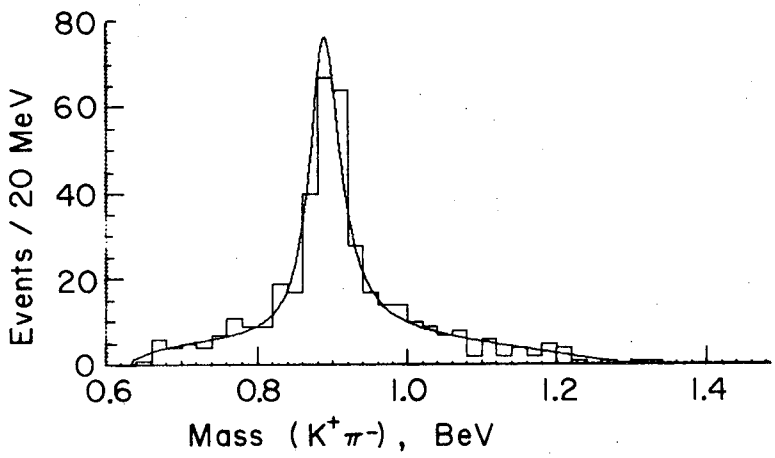

MUB-11444

Fig. 10 Mass scatterplot for the final state $K^+p\pi^+\pi^-$. Curves plotted on the mass histograms correspond to the production of K^*N^{*++}, K^{*0}, N^{*++}, and non-resonant background in proportions determined from a likelihood fit to the scatterplot distribution.

B. Production of K^*N^*

For our study of the reaction $K^+p \rightarrow K^{*o}N^{*++}$ we select those events for which $.85 < m_{K\pi^-} < .93$ and $1.12 < m_{p\pi^+} < 1.34$. By integrating separately the four terms in distribution 3 over this region of the triangle plot we estimate our sample to contain 82% K^*N^* events, 7% $K^*p\pi^+$, 7% $N^*K^+\pi^-$, and 4% non-resonant background, assuming no interference between these contributions. Using our estimate that the pion-produced background included in our total sample of events is less than 7%, and assuming that such events are distributed over the "triangle" plot roughly according to phase space, we may estimate that the number of π^+p events of type 2 included in the sample defined above is less than that 1/2% of that sample.

General expressions for the decay distributions of the K^* and N^* in terms of their spin density matrix elements were given in Section IV. We have evaluated those parameters for our sample of K^*N^* productions, using three parameter maximum likelihood fits to the decay distributions of the K^* and N^*, with the coordinate systems[8] defined in Figs. 11 and 12. Results are presented in Table IV for the total sample, and for subsamples corresponding to different regions of production angle. In Figs. 11 and 12 we present the decay distributions of the K^* and N^* respectively, along with curves determined by the density matrix elements obtained from our fit.

Table IV K^* and N^* density matrix parameters in the reaction $K^+p \rightarrow K^{*o} N^{*++}$, for various ranges of production angle θ.

K^*	$\cos\theta$	Δ^2	ρ_{00}	$\rho_{1,-1}$	$Re\rho_{10}$
	1.0 - .95	.13 - .19	0.90 ± 0.16	-0.22 ± 0.06	-0.18 ± 0.07
	.95- .90	.19 - .26	1.00 ± 0.12	0.14 ± 0.08	-0.18 ± 0.04
	.90- .80	.26 - .39	0.36 ± 0.12	-0.04 ± 0.10	-0.17 ± 0.06
	.80-(-1.)	.39 -2.68	0.58 ± 0.10	-0.08 ± 0.07	-0.10 ± 0.06
	1.0 -(-1.)	.13 -2.68	0.65 ± 0.06	-0.07 ± 0.04	-0.16 ± 0.04

N^*	$\cos\theta$	Δ^2	ρ_{33}	$Re\rho_{3,-1}$	$Re\rho_{31}$
	1.0 - .95	.13 - .19	0.24 ± .09	-0.01 ± 0.08	-0.10 ± 0.10
	.95- .90	.19 - .26	0.00 ± 0.11	0.07 ± 0.09	0.09 ± 0.09
	.90- .80	.26 - .39	0.26 ± 0.09	-0.06 ± 0.09	0.00 ± 0.10
	.80-(-1.)	.39 -2.68	0.18 ± 0.07	0.05 ± 0.07	-0.10 ± 0.08
	1.0 -(-1.)	.13 -2.68	0.18 ± 0.05	0.01 ± 0.04	-0.04 ± 0.05

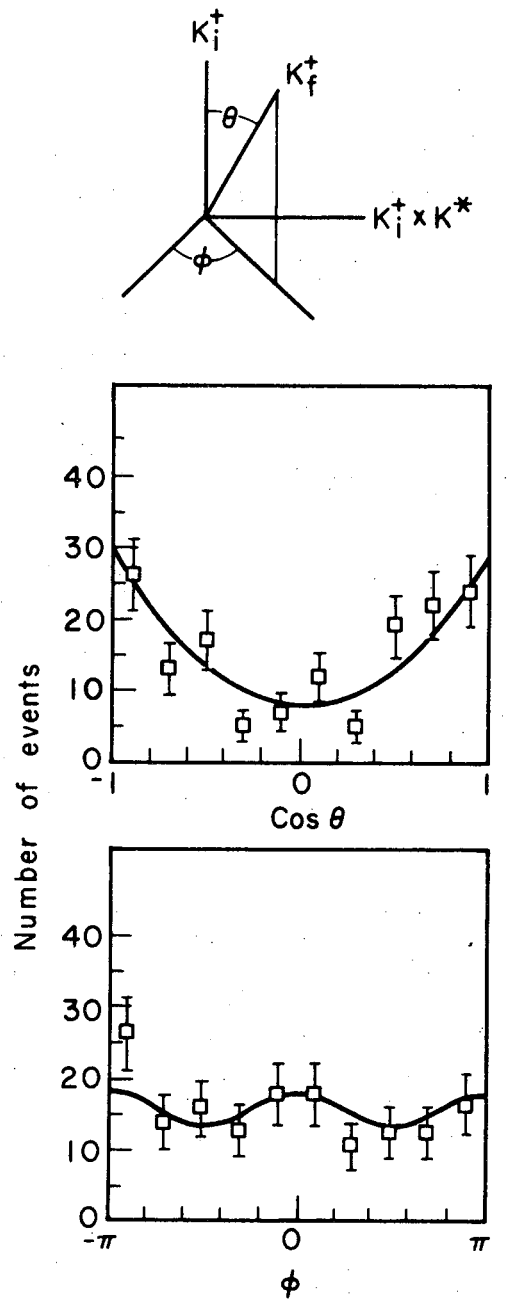

MUB-11442

Fig. 11 Decay angular distributions for the K^* in the channel $K^{*o}N^{*++}$. Particle symbols in the coordinate system diagram represent the direction of motion of the particles in the K^* rest frame. Curves are determined by K^* density matrix parameters obtained from a three parameter likelihood fit to the (θ,φ) distribution.

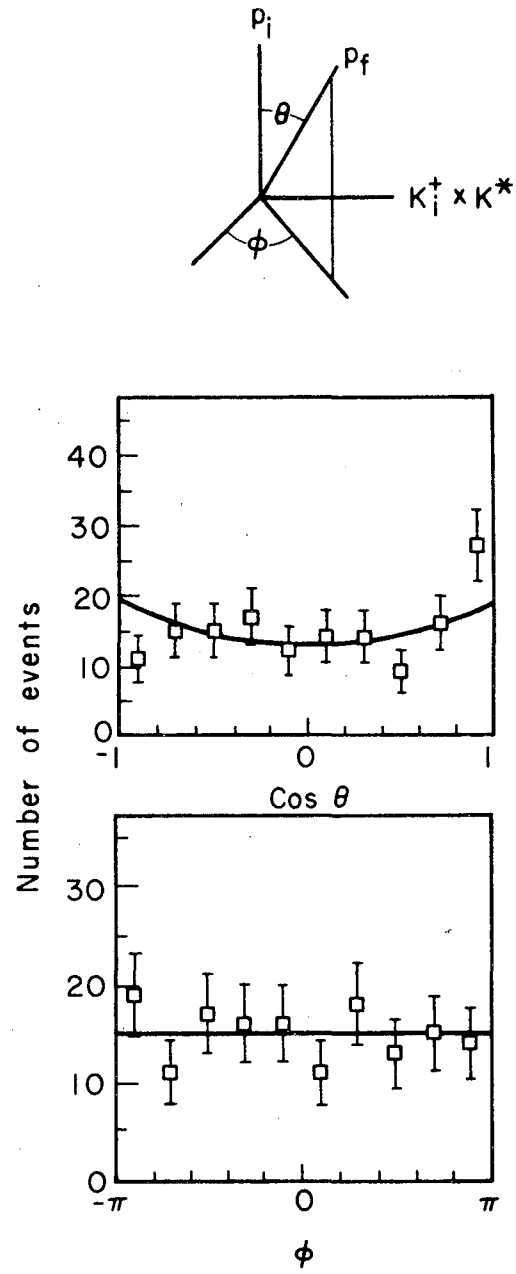

MUB-11441

Fig. 12 Decay angular distributions for the N^* in the channel $K^{*o}N^{*++}$. Particle systems in the coordinate system definition represent the direction of motion of the particles in the N^* rest frame. Curves are determined by N^* density matrix parameters obtained from a three parameter likelihood fit to the (θ,φ) distribution.

In Fig. 13 we present the K^*N^* production angular distribution for our sample. This distribution is sharply peaked with the K^* going forward, suggesting a peripheral process.

We note that the values of the K^* and N^* density matrix parameters for our sample are not far from being consistent with the predictions of an unmodified one pion exchange model, which requires that $\rho_{00} = 1$ while ρ_{1-1}, $\mathrm{Re}\rho_{10}$, ρ_{33}, $\mathrm{Re}\,\rho_{3,-1}$, and $\mathrm{Re}\rho_{31}$ all equal zero. Inclusion in this model of the effects of absorption in initial and final states can alter these predictions. Hence we now apply to our data an OME model, assuming pion exchange and including the effects of absorption.

The amplitude for the reaction $K^+p \to K^*N^*$ is given in the unmodified pion exchange model by[9]

$$M(t) = \frac{G^*}{m_\pi} \bar{U}_\mu(d)\, u(b)\, b^\mu \frac{1}{m_\pi^2 - t}\, g(a-e)\cdot\epsilon \qquad (4)$$

where a, b, d, and e represent respectively the four-momenta of the incident K^+, the target proton, the N^*, and the exchanged pion, m_π is the mass of the exchanged pion, t is the momentum transfer to the K^* $(t = -\Delta^2)$, and $U_\mu(d)$, $u(b)$, and ϵ are spinors corresponding, respectively, to the $N^*(J = 3/2)$, proton $(J = 1/2)$ and $K^*(J = 1)$. The $N^{*++}p\pi$ coupling constant G^* may be estimated from the N^* decay width $\Gamma_{N^*} = 120$ MeV to be $\frac{G^{*2}}{4\pi} \simeq .37$ and the $K^{*0}K^+\pi$ coupling constant g may be estimated from $\Gamma_{K^*} = 50$ MeV to be $\frac{g^2}{4\pi} = 1.67$. This amplitude

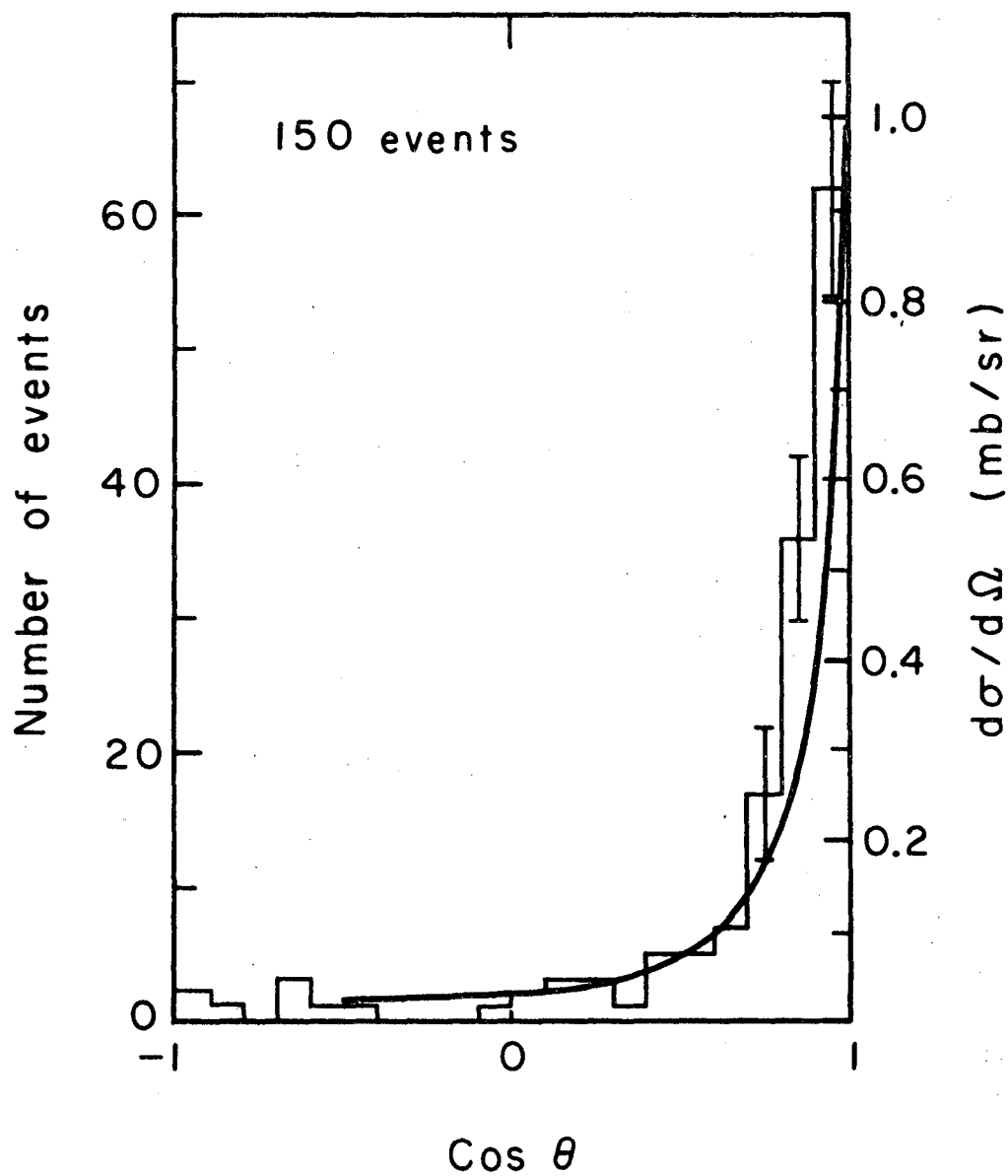

Fig. 13 Production angular distribution of the K^* in the reaction $K^+p \to K^{*o}N^{*++}$, $K^* \to K^+\pi^-$. The curve represents a pion exchange model modified only by a form factor.

MUB 11567

leads to a K^*N^* differential production cross section

$$\frac{d\sigma}{dt} = \frac{2}{3}\ \frac{\pi}{sq^2}\ \frac{g^2}{4\pi}\ \frac{G^{*2}}{4\pi m_\pi^{\ 2}}\left[(m_p+m_{N^*})^2 - t\right]\ \frac{a_c^{\ 2} b_d^{\ 2}}{(m_\pi^{\ 2}-t)^2} \qquad (5)$$

where s is the C.M. energy squared, q is the initial C.M. momentum, a_c is the momentum of the incident K^+ in the K^* rest frame, and b_d is the momentum of the incident proton in the N^* rest frame. This expression requires an additional factor of 2/3 to account for the branching ratio for the decay $K^{*o} \rightarrow K^+ \pi^-$.

Before proceeding to add absorption corrections we may ask how well the pion exchange model modified by a form factor alone can reproduce our data. A good fit to the K^*N^* production distribution at 1.96 BeV/c was obtained by multiplying expression (5) by a form factor

$$|F(t)|^2 = \left|\frac{\alpha^2 - m_\pi^{\ 2}}{\alpha^2 - t}\right|^2 \quad \text{with} \quad \alpha^2 = .165 \ .$$

Using this form factor we obtain the curve shown in Fig. 13. This curve reproduces the shape of the distribution fairly well, but is somewhat low in magnitude. The principle objections to this modification of the model are however the drastic and rather arbitrary form factor required to fit the data, and the fact that the modification fails to account for the deviations of the spin density matrices from the predictions of the unmodified model. In any case, it is unreasonable to expect that a channel such as K^*N^* production can be treated

without consideration of the effects of competing channels.

We turn then to the absorption model as formulated by Jackson[3,23] and others. We refer to the literature for a detailed discussion of the calculational methods and theoretical foundations for the model. Here we will only outline the method. The model begins with a partial-wave expansion for the unmodified (Born) meson exchange amplitudes, using a helicity formalism

$$< \lambda_{K^*}\lambda_{N^*}|B|\lambda_p > = \sum_j (j + \tfrac{1}{2}) < \lambda_{K^*}\lambda_{N^*}|T_j|\lambda_p > d^j_{\lambda\mu}(\theta) \qquad (6)$$

where λ_{K^*} , λ_{N^*} , and λ_p are the helicities of the corresponding particles, $\lambda = \lambda_p$ and $\mu = \lambda_{N^*} - \lambda_{K^*}$. Each term in the expansion is then multipled by an absorption factor $k(j) = e^{i\delta_j^+} e^{i\delta_j^-}$ where δ_j^+ and δ_j^- are the complex elastic-scattering phase shifts in the initial and final channels. In the model as formulated by Jackson, $e^{i\delta_j^\pm}$ is taken to be of the form

$$1 - C_\pm e^{-\gamma_\pm j^2}{}^{1/2}$$

where $C_+ = \sigma_T^{(+)}/4\pi A_+$ and $\gamma_+ = 1/2q^2 A_+$ where σ_T^+ is the total cross section for K^+p scattering, q is the incident C.M. momentum, and A is the parameter which appears in a parameterization of K^+p elastic scattering of the form

$$\frac{d\sigma_{e\ell}}{dt} \propto e^{At} \quad .$$

The quantities C_- and γ_- are defined analagously for the final state particles, but in practice are unknown. The derivation of the model requires $\delta_j^+ = \delta_j^-$, or else that the Born term interaction have a short range compared to the interactions which produce the absorption. The latter condition is certainly not satisfied for pion exchange, so that we are forced to hope that $C_+ = C_-$ and $\gamma_+ = \gamma_-$. In our calculation we will assume this to be true, although we also present the results of a calculation with $\gamma_- = 1/3\gamma_+$.

The Born helicity amplitudes appearing on the left of Eq. 6 are calculated from the amplitude of Eq. 4 using spinors corresponding to helicity states of the particles involved, paying careful attention to phases. There are 24 helicity amplitudes for K^*N^* production, of which only 12 are independent because of parity conservation. To make the expansion of Eq. 6 it is possible and convenient to divide each amplitude on the left into two parts, such that the partial wave expansion of one part can be approximated by an integral over Bessel functions, while the other part is easily expanded in terms of a very few low partial waves. The final expression for the modified amplitude is then, for small production angles,

$$M_n^{(i)} = A_n^{(i)} \int_{j_o}^{\infty} J_n(\omega x)\, K_n(\epsilon x)\, k(x - \tfrac{1}{2})x\, dx \qquad (7)$$

$$+ \sum_{j=j_o}^{j_{max}} \bar{A}_{n,j}^{(i)} \; d_{\lambda\mu}^{j}(\theta)\, k(j)$$

Here $M_n^{(i)}$ represents the modified helicity amplitude, where $n = |\lambda-\mu|$ and the index i distinguishes between amplitudes having the same value of n, J_n, and K_n denote ordinary and hyperbolic Bessel functions respectively, x is a variable corresponding to $j + \frac{1}{2}$, $j_o = \max(|\lambda|, |\mu|)$, $j_{max} = j_o$ or $j_o + 1$ in our case, θ is the C.M. scattering angle, $\omega = 2\sin\frac{\theta}{2}$, and ϵ is given by

$$qq'\epsilon^2 = m_\pi^2 + (q-q')^2 - \frac{1}{4s}\left[m_p^2 - m_{K^+}^2 - m_{N^*}^2 + m_{K^*}^2\right]^2$$

where q and q' are the magnitudes of the initial and final C.M. momenta. Equation 7 is essentially the same as Eq. 6 of reference 23, except that the latter equation includes only the term with $j = j_o$ in the sum over j. For K^*N^* production however, those amplitudes with $j_o = \frac{1}{2}$ include also a term with $j = \frac{3}{2}$ in this sum. Equation 6 of reference 23 also replaces $k(j)$ with $k(j - \frac{1}{2})$ in the sum over j. We will present results for both forms.

To evaluate C_+ and γ_+ for our calculation we use a total K^+p cross section of 17 mb.[26] Since analysis of K^+p elastic scattering is not yet complete for our experiment, we use a value of A_+ obtained by interpolating results at other energies,[27,28] obtaining $A_+ \approx 3.5$. We then obtain $C_+ = 1.0$ and $\gamma_+ = .15$, and put $C_- = C_+$, $\gamma_- = \gamma_+$.

In Fig. 14 we show the absorption model predictions for the K^*N^* production angular distribution near the forward direction,

compared with our experimental data. Curve a is the prediction of the unmodified OME model, while curve b is the prediction of the absorption model with the parameters defined above. Curve b reproduces the shape of the experimental distribution, but is about a factor of 2 too high in magnitude. For comparison we present curve c, which is the result of a calculation in which the range of the absorption in the final state has been increased by putting $\gamma_- = .05$, and curve d, which results from replacing $k(j)$ with $k(j - \frac{1}{2})$ in the sum of Eq. 7, following Jackson. In Fig. 15 we compare absorption model predictions with our data on the K^* and N^* density matrix parameters as a function of production angle. In each plot the solid curve corresponds to a calculation with $C_+ = C_- = 1.0$, $\gamma_+ = \gamma_- = .15$. Putting $\gamma_- = .05$ leads to curves almost identical to these. The dashed curves are the result of replacing $k(j)$ with $k(j - \frac{1}{2})$ in Eq. 7.

The agreement of the data on K^*N^* production with the predictions of the absorption model is not very good. However the model does roughly reproduce the production differential cross section, and succeeds generally in reproducing the sign and order of magnitude of the deviations of the density matrix parameters from the values predicted by the unmodified theory. A virtue of the model is that it involves no arbitrary parameters to be determined by "fitting".

One of the problems with the absorption model is the crude way in which the absorption factors must be represented as a function of j.

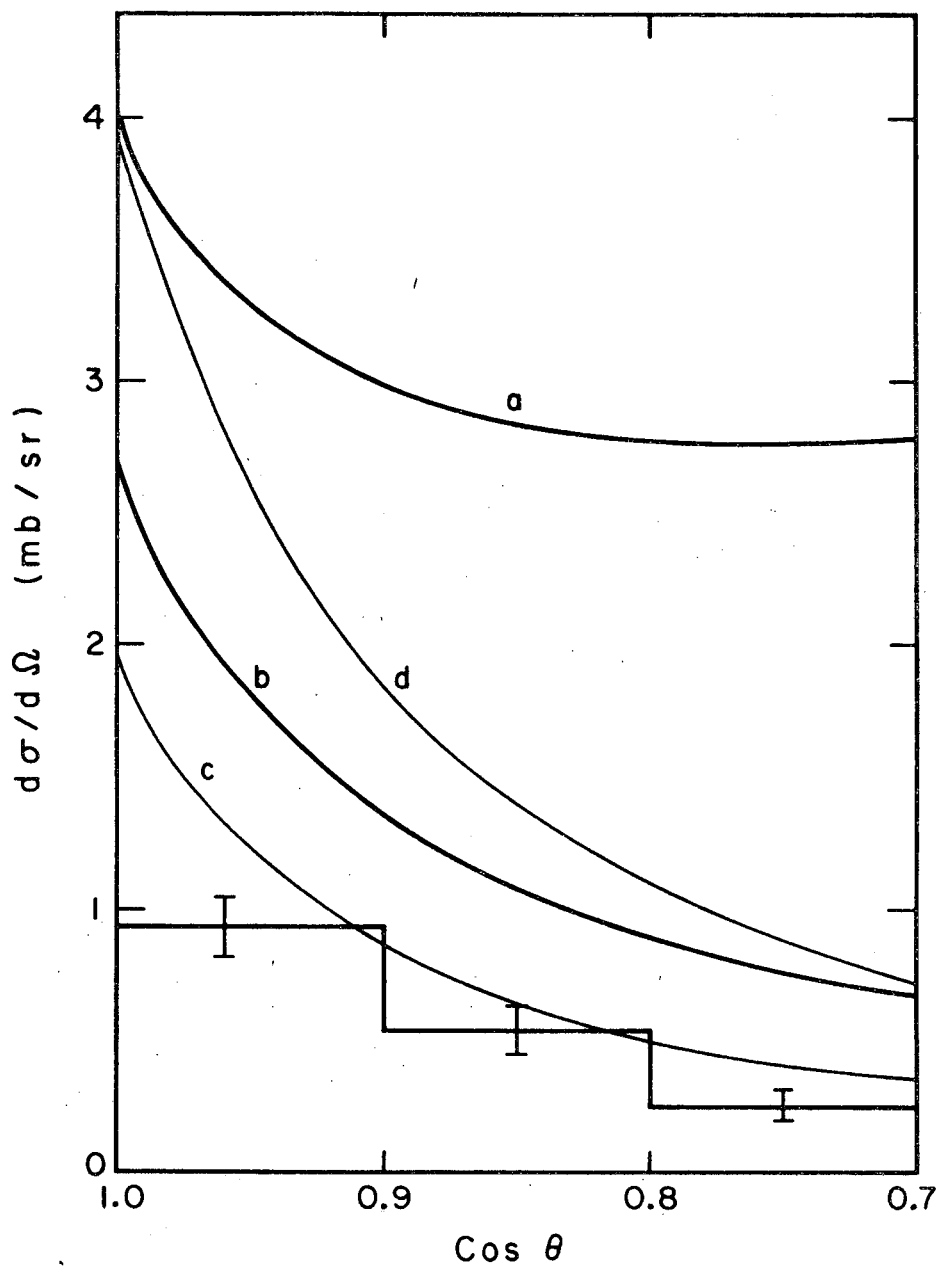

MUB-11569

Fig. 14 Production angular distribution of the K^* in the reaction $K^+p \to K^{*o} N^{*++}$; $K^* \to K^+\pi^-$. Curve a is the prediction of the unmodified pion exchange model; curves b , c , and d follow from π exchange modified by absorption as discussed in the text.

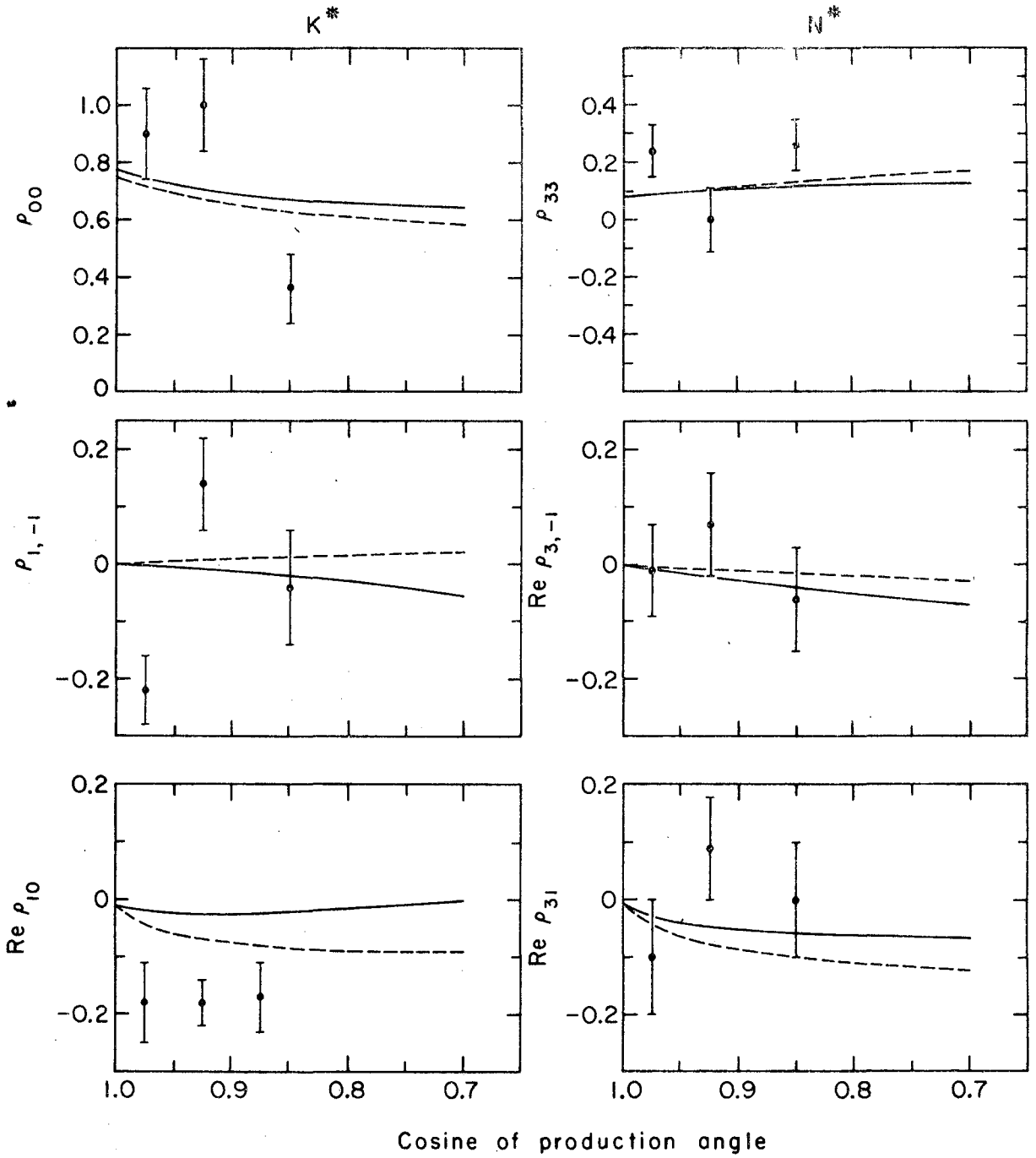

MUB-11570

Fig. 15 Density matrix parameters, as a function of production angle, for the K^* and N^* in the reaction $K^+p \rightarrow K^{*o}N^{*++}$. Curves are the predictions of an absorption model, as described in the text.

In fact, as pointed out by Jackson,[23] the absorption might more reasonably be taken to be a decreasing function of the orbital angular momentum ℓ . For the production of K^*N^* (or ρN^*) the values of ℓ can differ from the corresponding values of j by as much as 5/2, and the relations between ℓ and j are of course quite complicated. This may be a serious problem, since the results of absorption model calculations seem to be quite sensitive to the way that absorption is introduced in the low partial waves. This may be seen in comparing our results using $k(j)$ and $k(j - \frac{1}{2})$ in the sum of Eq. 7. This sensitivity has also been found, especially for production angular distributions, in a detailed study of some cases by Hogaasen et. al.[29]

VI. SEARCH FOR OTHER RESONANT STATES

We have examined all 2 and 3 body effective mass distributions in the channels

$$K^+p \rightarrow K^+p\ \pi^+\pi^- \qquad (400 \text{ events}) \qquad (8)$$

$$K^+p\ \pi^+\pi^-\pi^0 \qquad (\ 77 \text{ events}) \qquad (9)$$

and find no evidence for the production of resonant states other than $K^*(891)$, $N^*(1236)$, and ω . The cross section for ω production in channel 9 above is 0.07 ± 0.03 mb.

We have looked particularly for possible enhancements in the $K\pi\pi$ mass distributions in these channels. In Fig. 16 we show the $K^+\pi^+\pi^-$ mass distribution in channel 8. The dashed curve is the phase space distribution, while the solid curve is the distribution which would result from the production of K^{*0} and N^{*++} in the proportions indicated in section V, assuming simple Breit-Wigner forms for their production matrix elements, and assuming that these resonances decay isotropically. The experimental distribution deviates from both curves near 1.175 BeV. A sharp $K\pi\pi$ enhancement has been reported in π^-p reactions at this mass.[30] However that enhancement was found not to be associated with K^* production, while the peak in our distribution becomes more pronounced when we restrict the events to those with a $K^+\pi^-$ mass in the K^* region, shown in the shaded portion of Fig. 16. We find no evidence for a $K\pi\pi$ enhancement in this mass region in the events of channel 9. Hence we believe

that the $K^+ \pi^+ \pi^-$ enhancement in channel 8 is simply a kinematical reflection of the nonisotropic decay of the K^{*o} and N^{*++} produced in that channel.

The observation of a small peak in K^+p and K^+n total cross sections at a C.M. energy of about 1.91 BeV has raised the possibility of a $Y = 2$, $B = 1$, $I = 1$ resonant state with that mass and a width $\Gamma \approx 180$ MeV.[31] Hence we have examined the K^+p and $K^+p\pi$ distributions in the above channels for such an enhancement. We find no evidence for its production.

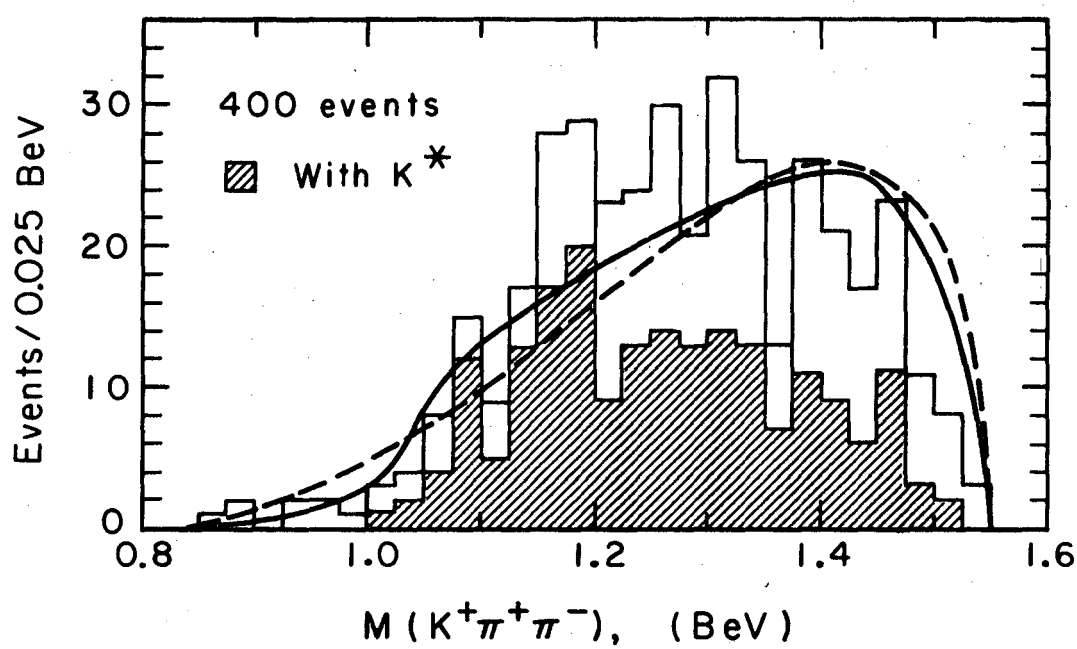

MUB 11568

Fig. 16 $M(K^+\pi^+\pi^-)$ distribution in the channel $K^+p\ \pi^+\pi^-$. The dashed curve is the phase space distribution, while the solid curve represents the effect of production of K^{*o} and N^{*++}, as described in the text.

VII. TEST OF SU_3 PREDICTIONS

We test here a set of relations of the form $\sum_i c_i A_i = 0$ relating amplitudes A_i for three body final states of K^+p reactions. These relations, whose derivation is discussed in Appendix C, are a consequence of exact SU_3 symmetry. They are

$$\sqrt{2}\, K^+ \pi^o p - K^o \pi^+ p - K^+ \pi^+ n = 0 \qquad (1)$$

$$K^+ K^o \Sigma^+ + K^o K^+ \Sigma^+ - \sqrt{2}\, K^+ K^+ \Sigma^o = 0 \qquad (2)$$

$$-K^+ \pi^o p + \sqrt{2}\, \pi^+ K^o p + \sqrt{3}\, K^+ \eta\, p + \sqrt{2}\, K^+ K^o \Sigma^+ = 0 \qquad (3)$$

$$2K^+ \pi^+ n + 2\pi^+ K^+ n - \sqrt{2}\, K^+ K^+ \Sigma^o + \sqrt{6}\, K^+ K^+ \Lambda = 0 \qquad (4)$$

Here we denote an amplitude by specifying the corresponding particles. Relations 1) and 2) above are a consequence of isotopic spin invariance alone.

First we must note that our relations imply inequalities of the form

$$\sum_{i \neq j} |c_i| \frac{\sigma_i(x)}{\rho_i(x)} \geq |c_j| \frac{\sigma_j(x)}{\rho_j(x)}$$

between differential channel cross sections $\sigma_i(x)$, where $\rho_i(x)$ is a phase space factor and we specify all momentum variables symbolically by x. However, because of limited data we would like to compare total channel cross sections. If the phase space factors were the same for all channels, as they would be for exact SU_3 symmetry, they could be removed from the inequality and one could derive corresponding inequalities:

$$\sum_{i \neq j} |c_i| \quad \sigma_i \geq |c_j| \quad \sigma_i$$

where $\sigma_i = \int \sigma_i(x)dx$. In comparing with experimental data we will apply these inequalities replacing σ_i with σ_i/ρ_i , thus approximating the effect of differing phase space by dividing each total channel cross section by a "total" phase space for that channel, defined by $\rho_i = \int \rho_i(x)dx$.

Since cross sections for the channels $K^+p\pi^o$ and $K^+\pi^+n$ have not yet been determined for our experiment, we will use the data at 3.0 BeV/c[32] to test the relations derived in Appendix C. At this higher energy the effects of differing phase space are considerably smaller. In Table V we list the relevant channel cross sections from reference 32, along with total phase space for each channel relative to the phase space for the channel $K^+p\pi^o$.

We now apply the inequalities implied by relations 1-4 above. Relation 1) implies a triangular inequality which is comfortably satisfied, the sides of the triangle having relative lengths of 1.83, 1.45, and .95. Relation 2) implies an inequality

$$\sqrt{\sigma(K^+K^o\Sigma^+)} \geq \sqrt{\sigma(K^+K^+\Sigma^o)}$$

which is also satisfied, the left and right sides having relative magnitude .27 and .19 respectively. Relation 3) is the first which is not implied by isotopic spin conservation alone, and is especially interesting since it relates strange particle production to non-strange

production. It implies a set of four inequalities, one of which is not satisfied. For the inequality with the channel $p\pi^+K^o$ on the right, the left and right sides have experimental magnitudes of 1.88 ± 0.17 and 2.04 ± 0.14. This inequality is satisfied within the errors however, and the magnitude of the violation is probably small compared to uncertainties in our method of making phase space corrections. Finally, relation 4) provides no useful inequalities among total channel cross sections.

We may conclude that the experimental data is consistent with the general predictions of SU_3 which we have applied. However these tests are not very stringent. Also, it is not clear how the effects of mass differences should be taken into account in applying these relations. It is possibly better to compare reaction channels not at the same C.M. energy, as we have done, but at C.M. energies giving the same Q value to each channel.[33] It will be interesting to apply these tests of SU_3 at very high energies, where effects of mass differences are minimized.

Table V. Three body channel cross sections and phase space factors for K^+p reactions at 3.0 BeV/c.[32]

	σ_i (mb)	ρ_i	$\sqrt{\sigma_i/\rho_i}$
$K^+\pi^o p$	1.7 ± .4	1.00	1.3
$K^o\pi^+ p$	2.1 ± .3	.99	1.45
$K^+\pi^+ n$	.9 ± .3	.99	.95
$K^+\eta p$	.006 ± .004	.46	.11
$K^+K^o\Sigma^+$	.015 ± .005	.21	.27
$K^+K^+\Sigma^o$	.0075± .0025	.21	.19
$K^+K^+\Lambda$	.023 ± .0045	.29	.28

ACKNOWLEDGMENTS

I am indebted and most grateful to Professor William Chinowsky, who has given me both guidance and freedom in excellent proportions.

I would like also to express deep gratitude to Dr. Jonas Schultz for many helpful discussions.

I thank Dr. William B. Johnson and Dr. Rudolf Larson, who shared the work on this experiment.

I thank also Mr. Julius Spiro, Dr. Hugh Brown, and the crew of the Brookhaven AGS accelerator, and Dr. Ralph Shutt and the crew of the Brookhaven bubble chamber group, for their part in this experiment.

I am grateful to Mr. Roger Bland for helpful discussions, and to Dr. Benjamin Shen and Mr. Victor Seeger for providing me with preliminary results of their work.

I thank Professor Emilio Segrè for his support of this work.

Many thanks are due to the scanners and measurers who worked on this experiment: Judy Conklin, Jean Freund, Gloria Tafralian, Teryl Pratt, Cathy Conner, Joyce Smart, and Carlis Braswell.

I appreciate also the contribution of Mrs. Rosemary Fowell in typing this thesis.

APPENDICES

A. Symmetry of the Spin Density Matrix

The spin density matrix is hermitian and satisfies $\mathrm{Tr}\,\rho = 1$. Parity conservation in the production process of a particle imposes on its spin density matrix additional conditions, whose form depends on the choice of coordinates, and in particular on whether the x, y, or z axis is taken to be $\hat{n}$, the perpendicular to the production plane. All three choices appear in the literature, and we collect here the corresponding conditions on ρ

$\hat{n}$	symmetry condition
$\hat{x}$	$\rho_{mm'} = \rho_{-m,-m'}$
$\hat{y}$	$\rho_{mm'} = (-1)^{m-m'}\,\rho_{-m,-m'}$
$\hat{z}$	$\rho_{mm'} = (-1)^{m-m'}\,\rho_{mm'}$

In each case z is taken to be the axis of quantization. These conditions hold only if in the initial state of the reaction the polarization, if any, is along the normal to the production plane. If this is so the conditions on ρ may be derived by noting that since the initial state is invariant under reflection in the production plane, therefore the final state is similarly invariant, in the sense that the reflected state is equally probable. If we sum over all the other spins and momenta that distinguish up from down in the final state, (but not necessarily over momentum transfer to the particle considered), then we may require the spin density matrix of the particle to be

invariant under reflection in the production plane. Now reflection = RP where P is the parity operation and R is a rotation by π around $\hat{n}$. P leaves ρ invariant, since it is bilinear in ψ, and invariance under the rotation then requires

$$\rho_{mm'} = D^{J\dagger}_{mn}\, \rho_{nn'}\, D^{J}_{n'm'} \qquad (1)$$

where D^J is the rotation matrix for angle π about $\hat{n}$. J is the spin of the particle. The form of D^J depends on the choice of axes as follows:

$\hat{n}$	D_{mn}
$\hat{x}$	$D_{mn}(\frac{-\pi}{2}, \pi, \frac{\pi}{2}) = e^{i\frac{\pi}{2}(m-n)}(-1)^{J-n}\,\delta_{m,-n}$
$\hat{y}$	$D_{mn}(0, \pi, 0) = (-1)^{J-n}\,\delta_{m,-n}$
$\hat{z}$	$D_{mn}(0,0,\pi) = e^{-i\pi n}\,\delta_{mn}$

Substituting these expressions for D^J in equation (1) then gives the symmetry conditions on ρ given above. Note that the form of the condition depends only on the axis chosen to be normal to the production plane, and not on the orientation of the other two axes in that plane. In particular, the form for $\hat{n} = \hat{y}$ is correct both for helicity coordinates, in which $\hat{z}$ is taken to be the direction of motion of the particle, and for the often useful coordinates in which $\hat{z}$ is taken to be the direction of an incident particle in the rest frame of the outgoing particle.

B. Covariant $J = 3/2$ Spin-Energy Projection Operator

In performing calculations involving a spin 3/2 particle such as the $N^*(1236)$ it is often possible to reduce spin sums to trace calculations by introducing a spin-energy projection operator. Such an operator is used by Jackson[9] and other authors to whom he refers. We present here a derivation of that operator in a somewhat different form which we find particularly convenient to use.[34]

We want a projection operator which projects out the positive energy, $J = 3/2$ part of a product of a Dirac spinor and a four-vector:

$$P = P^{3/2}\, P^{1}\, \Lambda_+$$

where

$$\Lambda_+ = \frac{\not{p}+m}{2m}$$

is the positive energy projection operator acting on the spinor,

$$P^{1}_{\mu\nu} = -g_{\mu\nu} + \frac{p_\mu p_\nu}{m^2}$$

projects out the $J = 1$ part of the four-vector, and $P^{3/2}$ is the $J = 3/2$ projection operator acting on an $E > 0$ spinor and $J = 1$ four-vector. Here m and p_μ are the mass and four-momentum of the particle described, and $g_{00} = +1$. To construct $P^{3/2}$ we start in the particle rest frame, where we have

$$\begin{aligned} P^{3/2}_{ij} &= \frac{2}{3}\,(1 + J_1 \cdot J_2)_{ij} \\ &= \frac{2}{3}\,(\delta_{ij} - \frac{i}{2}\,\epsilon_{ijk}\,\sigma^k) \end{aligned}$$

where we have used

$$(J_1)^k_{ij} = - i \epsilon_{ijk}$$

and

$$J_2^k = \frac{\sigma^k}{2}$$

We now cast this in the covariant form

$$P^{3/2}_{\mu\nu} = \frac{2}{3} (g_{\mu\nu} - \frac{i}{2m} \epsilon_{\mu\nu\rho\sigma} \gamma^\rho \gamma^5 p^\sigma)$$

where

$$\epsilon_{0123} = +1 .$$

We note here that the three projection operators $P^{3/2}$ P^1 $\Lambda+$ commute with each other. Finally we combine them to get

$$P_{\mu\nu} = \frac{2}{3} (\not{p}+m)(-g_{\mu\nu} + \frac{1}{m^2} p_\mu p_\nu + \frac{i}{2m} \epsilon_{\mu\nu\rho\sigma} \gamma^\rho \gamma^5 p^\sigma)$$

where we have dropped a factor of $\frac{1}{2m}$ so that products $U_\mu U_\nu$ may be replaced by $P_{\mu\nu}$ in performing spin sums in calculations involving Rarita-Schwinger $J = 3/2$ spinors normalized $\bar{U}_\mu U^\mu = 2m$.

The above expression may also be cast in the form given by Jackson, expressed here with our conventions

$$P_{\mu\nu} = (\not{p}+m)\left[-g_{\mu\nu} + \frac{2}{3m^2} p_\mu p_\nu + \frac{1}{3} \gamma_\mu \gamma_\nu + \frac{1}{3m} (\gamma_\mu p_\nu - \gamma_\nu p_\mu)\right]$$

The first form is particularly convenient to use in trace calculations however, since all γ matrices are in the single term $\epsilon_{\mu\nu\rho\sigma} \gamma^\rho \gamma^5 p^\sigma$, and the antisymmetry in $\mu\nu$ and/or the γ^5 in this term kill instantly most terms in the trace which involve it. Typical terms remaining are

of the form $\mathrm{Tr}\, \not{A}\not{B}\not{C}\not{D}\, \gamma^5$ where $\not{D}\gamma^5$ comes from the $\epsilon_{\mu\nu\rho\sigma}\gamma^\rho \gamma^5 p^\sigma$ term, and particular $D_\rho = \epsilon_{\rho\mu\nu\sigma} E^\mu F^\nu p^\sigma$. This is easily evaluated using $\mathrm{Tr}\, \not{A}\not{B}\not{C}\not{D}\, \gamma^5 = 4i\, \epsilon_{\alpha\beta\gamma\delta} A^\alpha B^\beta C^\gamma D^\delta$ and

$$\epsilon_{mnqp}\, \epsilon^{mrst} = \delta_n^s \delta_q^r \delta_p^t + \delta_n^r \delta_q^t \delta_p^s + \delta_n^t \delta_q^s \delta_p^r$$

$$-\delta_n^r \delta_q^s \delta_p^t - \delta_n^s \delta_q^t \delta_p^r - \delta_n^t \delta_q^r \delta_p^s .$$

C. Derivation of Cross Section Relations from Reaction Symmetries

a. General Method

It often happens that a symmetry such as SU_2 or SU_3 can be used to relate a number m of amplitudes A_i for reaction channels to a smaller number n of amplitudes a_i which are characteristic of the symmetry. Thus, $A_i = M_{ij} a_j$ where M is an $m \times n$ matrix determined by the symmetry. From these relations one may derive a set of relations of the form $\sum_i c_i A_i = 0$. The number of independent relations of this sort obtainable without any knowledge of the a_i is $m-r$, where r is the rank of the matrix M. Each such relation provides a set of inequalities of the sort $\sum_{i \neq j} |C_i||A_i| \geq |C_j||A_j|$ which may be experimentally tested using $|A_i| = \sqrt{\sigma_i/\rho_i}$ where σ_i is the corresponding channel differential cross section and ρ_i is a phase space factor.

A simple example is provided by the three reaction channels

$$K^+ p \to K^+ \; p \; \pi^0 \qquad 1)$$

$$K^+ \; n \; \pi^+ \qquad 2)$$

$$K^0 \; p \; \pi^+ \qquad 3)$$

whose amplitudes are related by isotopic spin conservation to two amplitudes corresponding to coupling the pion and nucleon in a $I = \frac{1}{2}$ or $3/2$ state:

$$\begin{pmatrix} A_1 \\ A_2 \\ A_3 \end{pmatrix} = \begin{pmatrix} 1 & 1/\sqrt{2} \\ \sqrt{2} & -1/2 \\ 0 & 3/2 \end{pmatrix} \begin{pmatrix} a_1 \\ a_3 \end{pmatrix}$$

This yields the single relation $\sqrt{2}\, A_1 - A_2 - A_3 = 0$.

For relations involving many amplitudes, extracting all possible amplitude sum rules can become quite tedious and confusing. It is possible however to extract methodically and simply all independent amplitude relations from expressions of the form $\vec{A} = M \; \vec{a}$ by using the following method. The method is similar to one which is commonly used to invert square matrices. We start with our relation written $I \; \vec{A} = M \; \vec{a}$, where I is the $m \times m$ identity matrix. We then perform a series of elementary row operations on the $m \times n$ matrix M , while simultaneously performing the same operations on the matrix I on the left. An elementary row operation is one of the following: 1) multiplication of a row by a non-zero constant, 2) addition of a multiple of one row to another row, or 3) interchange of two rows. Noting that

each such operation corresponds to multiplication from the left by a simple matrix, we see that the above equality is preserved at each step as I evolves into a new matrix E . The object is to produce rows of zeros in the matrix M . For each such row achieved, the corresponding row of E clearly provides the coefficients of a sum rule relating the A_i . Elementary row operations do not change the rank of a matrix, so that all the rows of the matrix E are linearly independent at every step. Hence all the amplitude relations generated with this method are independent.

In principle one can reduce the matrix M methodically by using a row to produce m-1 zeros in the first column, another row to produce m-1 zeros in the second column, and so on. In practise however M usually has a quite simple form, and one can easily spot operations which quickly generate rows of zeros. One proceeds until it is clear that the remaining non-zero rows are all linearly independent, at which point the maximum number of independent amplitude relations has been derived.

One might postulate that certain of the amplitudes a_i are zero. Then one may eliminate the corresponding columns in M and proceed as before, obtaining in general a greater number of amplitude relations. In our example above one might postulate that only the $I = 3/2$ coupling of the $N\pi$ system contributes--e.g., perhaps the reaction proceeds only by way of N^*_{33} production.

To provide a useful test of a symmetry, an amplitude relation

should involve only channels which are experimentally measurable, and should relate a minimum of amplitudes so that the corresponding cross section inequalities impose as stringent a condition as possible. From a given set of amplitude relations it is possible to derive new ones which, while not independent of the original relations, may be more useful in practise. This is conveniently done at this point by collecting the sum rule rows of E into an $(m-r) \times m$ matrix which is then manipulated using elementary row operations in order to produce a minimum number of non-zero elements in each row, and a minimum number of non-zero elements in each column corresponding to a reaction channel about which no information is available.

b. <u>SU_3 Symmetry of $K^+ p \to PPB$</u>

We consider now the relations implied by exact SU_3 symmetry for $K^+ p$ three body final states of the sort PPB, where each P is a member of the pseudoscaler octet $(K, \bar{K}, \pi, \eta)$, and B is a member of the baryon octet $(N, \Xi, \Sigma, \Lambda)$. There are seven distinct channels of this sort, corresponding to twelve final states when we treat e.g., $K^+ \pi^o p$ and $\pi^o K^+ p$ as distinct final states, which makes sense when spatial wave functions are associated with the particles. The final states are:

$$K^+ p \to K^+ \pi^o p \quad , \quad \pi^o K^+ p$$
$$K^o \pi^+ p \quad , \quad \pi^+ K^o p$$
$$K^+ \eta \; p \quad , \quad \eta \; K^+ p$$

$K^+ \pi^+ n$, $\pi^+ K^+ n$

$K^+ K^o \Sigma^+$, $K^o K^+ \Sigma^+$

$K^+ K^+ \Sigma^o$

$K^+ K^+ \Lambda$

The initial state $K^+ p$ transforms like the $I = I_3 = 1$, $Y = 2$ member of the 27 dimensional representation of SU_3 . Amplitudes for the twelve final states may then be related to six amplitudes, corresponding to six possible ways of coupling three octets to get a 27. Using a tensor representation of the octets, one may chose six amplitudes a_i corresponding to the 6 permutations of the particle labels 1, 2, 3 in the coupling

$$\psi_1^{\alpha}(1) \quad \psi_{\alpha}^{3}(2) \quad \psi_1^{3}(3) .$$

In each permutation $\psi(1)$ is the tensor which represnts the first meson, $\psi(2)$ represents the second meson, and $\psi(3)$ represents the baryon. The first such coupling, for no permutation of 1-2-3, is

$$\frac{1}{\sqrt{6}} \eta K^+ p + \frac{1}{\sqrt{2}} \pi^o K^+ p + \pi^+ K^o p - 2 K^+ \eta p .$$

The remaining five couplings are then obtained immediately by permuting particle labels and substituting $K \leftrightarrow N$, $\pi \leftrightarrow \Sigma$, $\eta \leftrightarrow \Lambda$ when baryon and meson labels are interchanged. For example, the coupling for the permutation 1-3-2 is

$$\frac{1}{\sqrt{6}} \eta K^+ p + \frac{1}{\sqrt{2}} \pi^o K^+ p + \pi^+ K^+ n - 2 K^+ K^+ \Lambda .$$

The coefficients of the physical channels in these six couplings then form the elements of the 12×6 matrix M in an expression $\vec{A} = M\vec{a}$. This matrix has a simple form, and is easily reduced with the method described in the preceeding section to yield relations 1 - 4 in Section VII of this thesis.

These relations are also easily derived in a direct way using I-spin and U-spin coupling schemes. However, the method described here is equally easy and has several advantages. It assures that all possible relations will be found, that they are all independent, and that the phases of the amplitudes involved are all consistent so that the relations may be combined to yield new forms. Further, with an appropriate choice of the amplitudes a_i it is easy to feed in possible assumptions about the dominance of certain couplings--for example, that the baryon and one meson couple predominantly through a channel corresponding to the $J^P = 3/2^+$ decuplet.

FOOTNOTES AND REFERENCES

1. N. J. Sopkovich, Nuovo Cimento 26, 186 (1962).

2. L. Durand and Y. T. Chiu, Phys. Rev. 139, B646 (1965).

3. K. Gottfried and J. D. Jackson, Nuovo Cimento 34, 735 (1964).

4. C. Baltay, J. Sandweiss, J. Sanford, H. Brown, M. Webster, and S. Yamamoto, Nucl. Instr. Methods 20, 37 (1963); J. Leitner, G. Moneti, and N. P. Samios, ibid. 20, 42 (1963).

5. W. E. Humphrey and A. H. Rosenfeld, Ann. Rev. Nucl. Sci. 13, 103 (1965); A. H. Rosenfeld, UCRL-9099 (1961), Lawrence Radiation Laboratory, Berkeley.

6. G. Trilling, UCRL-16473 (November, 1965).

7. D. Berley and N. Gelfand, Phys. Rev. 139, B1097 (1965).

8. It should be noted that the sign of the density matrix parameter $\mathrm{Re}\rho_{10}$ for the K^* and $\mathrm{Re}\rho_{31}$ for the N^* depends on the choice of the normal to the production plane. We take always $\hat{n} = (\widehat{q \times q'})$ where q is the momentum of the incident K^+, and q' is the momentum of the K^* in the final states K^*p and K^*N^*, or of the K^o in the final state K^oN^*.

9. J. D. Jackson and H. Pilkuhn, Nuovo Cimento 33, 906 (1964); 34, 1841E (1964).

10. S. Goldhaber, J. L. Brown, I. Butterworth, G. Goldhaber, A. A. Hirata, J. A. Kadyk, and G. H. Trilling, Phys. Rev. Letters 15, 737 (1965).

11. J. B. Bronzan and F. E. Low, Phys. Rev. Letters 12, 522 (1964).

12. M. Ferro-Luzzi, R. George, Y. Goldschmidt-Clermont, V. P. Henri, B. Jongejans, D. W. G. Leith, G. R. Lynch, F. Muller and J.-M. Perreau, Nuovo Cimento 36, 1101 (1965).

13. S. Goldhaber, W. Chinowsky, G. Goldhaber, and T. O'Halloran, Phys. Rev. 142, 913 (1966).

14. G. Goldhaber, W. Chinowsky, S. Goldhaber, W. Lee, and T. O'Halloran, Phys. Letters 6, 62 (1963).

15. M. Ferro-Luzzi, R. George, Y. Goldschmidt-Clermont, V. P. Henri, B. Jongejans, D. W. G. Leith, G. R. Lynch, F. Muller, and J.-M. Perreau, Nuovo Cimento 39, 417 (1965).

16. M. G. Bowler, R. W. Bland, J. L. Brown, G. Goldhaber, J. A. Kadyk, V. Seeger, and G. H. Trilling; Paper presented at the Oxford International Conference on Elementary Particles (1965), and UCRL-16370 (December, 1965), Lawrence Radiation Laboratory, Berkeley.

17. E. Boldt, J. Duboc, N. H. Duong, P. Eberhard, R. George, V. P. Henri, F. Levy, J. Poyen, M. Pripstein, J. Cussard, and A. Tran, Phys. Rev. 133, B220 (1964).

18. G. B. Chadwick, D. J. Crennell, W. T. Davies, M. Derrick, J. H. Mulvey, P. B. Jones, D. Radojicic, C. A. Wilkinson, A. Bettini, M. Cresti, S. Limentani, L. Peruzzo, and R. Santangelo, Phys. Letters 6, 309 (1963). See also Ref. 12 and references given therein.

19. B. Kehoe, Phys. Rev. Letters 11, 93 (1963).

20. V. Seeger, (Lawrence Radiation Laboratory, Berkeley), private communication.

21. The value of ρ_{oo} at $P_{Lab} = 1.45$ BeV/c in Fig. 8 is based on an estimate of the pseudoscalar exchange contribution given in Ref. 18.

22. B. Shen, (Lawrence Radiation Laboratory, Berkeley), private communication.

23. J. D. Jackson, J. T. Donohue, K. Gottfried, R. Keyser, and B. E. Y. Svensson, Phys. Rev. 139, B428 (1965).

24. H. Högaasen and J. Högaasen, Nuovo Cimento 39, 941 (1965).

25. C. Alff-Steinberger, D. Berley, D. Colley, N. Gelfand, D. Miller, U. Nauenberg, J. Schultz, T. H. Tan, H. Brugger, P. Kramer, and R. Plano, Phys. Rev. 145, 1072 (1966).

26. V. Cook, D. Keefe, L. T. Kerth, P. G. Murphy, W. A. Wenzel, and T. F. Zipf, Phys. Rev. Letters 7, 182 (1961).

27. W. Chinowsky, G. Goldhaber, S. Goldhaber, T. O'Halloran, and B. Schwarzschild, Phys. Rev. 139, B1411 (1965).

28. J. Debaisieux, F. Grard, J. Heughebaert, L. Pape, R. Windmolders, R. George, Y. Goldschmidt-Clermont, V. P. Henri, D. W. G. Leith, G. R. Lynch, F. Muller, J.-M. Perreau, G. Otter, and P. Sällström, Nuovo Cimento 43, A142 (1966).

29. H. Högaasen, J. Högaasen, R. Keyser, and B. E. Y. Svensson, Nuovo Cimento 42, A323 (1966).

30. T. P. Wangler, A. R. Erwin, W. D. Walker, Phys. Letters 9, 71 (1964); D. H. Miller, A. Z. Kovacs, R. L. McIlwain, T. R. Palfrey, and G. W. Tautfest, Phys. Letters 15, 74 (1965).

31. R. L. Cool, G. Giacomelli, T. F. Kycia, B. A. Leontic, K. K. Li, A. Lundby, and J. Teiger, Phys. Rev. Letters 17, 102 (1966).

32. M. Ferro-Luzzi, R. George, Y. Goldschmidt-Clermont, V. P. Henri, B. Jongejans, D. W. G. Leith, G. R. Lynch, F. Muller, and J.-M. Perreau, Proceedings of the Sienna International Conference on Elementary Particles (1963), and D. W. G. Leith, private communication.

33. See for example S. Meshkov, G. A. Snow, and G. B. Yodh, Phys. Letters 12, 87 (1964).

34. A form like the one derived here is presented by G. Mohan and S. C. Agarwal, Nuovo Cimento 37, 430 (1965), who credit it to C. Zemach, Proceedings of the Summer School on High Energy Physics at Kodaikanal, South India. I thank Dr. J. D. Jackson for bringing this to my attention.

This report was prepared as an account of Government sponsored work. Neither the United States, nor the Commission, nor any person acting on behalf of the Commission:

A. Makes any warranty or representation, expressed or implied, with respect to the accuracy, completeness, or usefulness of the information contained in this report, or that the use of any information, apparatus, method, or process disclosed in this report may not infringe privately owned rights; or

B. Assumes any liabilities with respect to the use of, or for damages resulting from the use of any information, apparatus, method, or process disclosed in this report.

As used in the above, "person acting on behalf of the Commission" includes any employee or contractor of the Commission, or employee of such contractor, to the extent that such employee or contractor of the Commission, or employee of such contractor prepares, disseminates, or provides access to, any information pursuant to his employment or contract with the Commission, or his employment with such contractor.